

Study of the acoustical performance of lightweight floors

Master's Thesis in the Master's programme in Sound and Vibration

RAÚL PAGÁN MUÑOZ

Department of Civil and Environmental Engineering

Division of Applied Acoustics

Vibroacoustics Group

CHALMERS UNIVERSITY OF TECHNOLOGY

Göteborg, Sweden 2011

Master's Thesis 2011:88

MASTER'S THESIS 2011:88

Study of the acoustical performance of lightweight floors

Master's Thesis in the Master's programme in Sound and Vibration

RAÚL PAGÁN MUÑOZ

Department of Civil and Environmental Engineering

Division of Applied Acoustics

Vibroacoustics Group

CHALMERS UNIVERSITY OF TECHNOLOGY

Göteborg, Sweden 2011

Study of the acoustical performance of lightweight floors

Master's Thesis in the Master's programme in Sound and Vibration
RAÚL PAGÁN MUÑOZ

© RAÚL PAGÁN MUÑOZ, 2011

Master's Thesis 2011:88
Department of Civil and Environmental Engineering
Division of Applied Acoustics
Vibroacoustics Group
Chalmers University of Technology
SE-412 96 Göteborg
Sweden
Telephone: + 46 (0)31-772 1000

Cover:
Eigenfrequency deformation plot of a lightweight floor.

Department of Civil and Environmental Engineering

Göteborg, Sweden 2011

To my wife...

Study of the acoustical performance of lightweight floors

Master's Thesis in the Master's programme in Sound and Vibration

RAÚL PAGÁN MUÑOZ

Department of Civil and Environmental Engineering

Division of Applied Acoustics

Vibroacoustics Group

Chalmers University of Technology

ABSTRACT

During the last decades, new building techniques based on lightweight systems have been developed and today they are frequently used in many countries. Since lightweight construction is a relatively new building technique, most of the acoustics regulations are still based on traditional building technology where heavyweight materials are mainly used. This has been shown to be a problem basically because the acoustic rating of a structure using the standard methods is not always well correlated with the perceived disturbances. The Thesis work pretends to clarify the vibrational behaviour of the lightweight floors at very low frequencies focusing only on the first order modes. The Waveguide Finite Element Method (WFEM) has been applied in order to study from a "wave's" point of view using the dispersion relations plots as one of the main analysis tools. This approach is very helpful to facilitate the physical understanding of the vibrational performance of the floors. Two simple models have been built, a wooden and a concrete floor, in order to compare the wave field and the mobilities of a lightweight and a heavyweight floor. Additionally, the work includes a parameter study to analyze the influence of how certain parameters of the lightweight model influence its vibrational performance. The sound radiation of the structure is studied using baffle plane radiator and the Rayleigh integral.

Key words: acoustics, vibration, radiation, waveguide, FEM, dispersion relation, lightweight floors, wooden floors, wave propagation, modes, mobility, periodic structure, pass-band, stop-band.

Contents

ABSTRACT	I
CONTENTS	III
PREFACE	IV
1 INTRODUCTION	1
1.1 Waveguide Finite Element Method	2
1.1.1 Fundamentals	2
1.1.2 Methodology	4
1.2 Sound radiation	5
2 MODELS	8
2.1 Finite Element resolution	8
2.2 Heavyweight floor (HWF)	11
2.3 Lightweight floor (LWF)	12
2.4 Wave field analysis	14
2.4.1 Interpretation of the dispersion diagrams	14
2.4.2 Analysis of the deformation diagrams	17
2.5 Mobility analysis	24
3 VALIDATION	26
4 PARAMETER STUDY	29
4.1 Material's elastic constants analysis (PS_1)	30
4.2 Geometry analysis (PS_2)	31
4.2.1 Scenario PS_2.1	31
4.2.2 Scenario PS_2.2	33
4.3 Pass-band / Stop-band effect	34
5 SOUND RADIATION	37
6 CONCLUSIONS	40
7 FUTURE WORK	42
8 REFERENCES	43
APPENDIX A. DISPERSION RELATIONS FREQUENCIES	44
APPENDIX B. WFEM / FEM DEFORMATION PLOTS	45
APPENDIX C. PS_1 DETAILED ANALYSIS	51

Preface

This work has been done as part of the Master's programme in Sound and Vibration. The scheme of the work was proposed by Professor Wolfgang Kropp who has been the Supervisor of the study. The work has been done since July 2010 inside the Vibroacoustics Group at the Division of Applied Acoustics (Department of Civil and Environmental Engineering) of Chalmers University of Technology.

The Thesis work pretends to clarify the vibrational behaviour of the lightweight floors at very low frequencies. The study has focused in the first order modes. The Waveguide Finite Element Method (WFEM) has been applied in order to study from a "wave's" point of view using the dispersion relations plots as one of the main analysis tools. This approach is very helpful to facilitate the physical understanding of the vibrational performance of the floors.

Two simple models have been built, a wooden and a concrete floor, in order to compare the wave field and the mobilities of a lightweight and a heavyweight floor. The results of the models using WFEM have been validated using a normal FEM approach. The initial plan was to validate the results using measurements on a real floor but after two frustrated tries the idea was discarded.

The initial project goals were adapted as the first results were obtained and analyzed. We decided to include a parameter study to analyze the influence of some properties of the lightweight model in its vibrational performance.

The sound radiation of the structure is studied using the baffle plane radiator and the Rayleigh integral.

Finally, I would like to thank the people that have made this possible; they know who they are...

Göteborg June 2011

Raúl Pagán Muñoz

1 Introduction

During the last decades, new building techniques based on lightweight systems have been developed and today they are frequently used in many countries. These systems are made of lightweight panels and beams, and they are often more environmentally friendly than other traditional techniques. Moreover, the lightweight materials are easier to transport and store reducing the overall cost of the process. Among other, these are some of the reasons why this building technique is getting more and more popular.

One of the most extended materials used in lightweight buildings is wood and timber related products. This work is focused on a wooden floor.

Since using lightweight construction in wood is a relatively new building technique, most of the acoustics regulations are still based on traditional methods using concrete and other heavyweight materials. This has been shown to be a problem, Hagberg (2005) (1) basically because the acoustic rating of a structure using the standard methods (p.e., ISO 140-7 (1998)(2)) is not always well correlated with the perceived disturbances caused by footsteps, falling masses, etc. Specifically, wooden houses were known for their poor impact sound insulation, fulfilling requirements but highly annoying, Sjökvist (2008) (3).

This work is mainly focused on impact sound isolation at low frequencies (the frequency range of interest is from 0 to 200 Hz) where the problem is more noticeable. The goal of the project is to get a better understanding of the acoustical performance of these structures. To achieve this a numerical method is used to simulate and compare the vibrational field of a lightweight floor (LWF) and a heavyweight floor (HWF). The first part of the work concerns the design of a model for a wooden and a concrete floor using the Waveguide Finite Element Method (WFEM).

WFEM can be used for structures with constant geometrical and elastic properties in one direction referred as waveguide (X-direction in this study). Traditional Finite Element Method (FEM) is used to solve the dynamic behaviour of the structure's cross-section while the vibrational performance of the whole system is described in terms of waves along the waveguide using sine functions to introduce the simply supported conditions at the X-dimension boundaries of the floor. WFEM can be considered a combination of several modelling techniques, Sjökvist (2008) (3). The modal approach is used to calculate the mobilities of the structures.

The models and their results are described, analyzed and compared in Chapter 2. Moreover, a validation of the model is presented in Chapter 3.

A parameter study for the LWF is carried out in order to understand how different parameters influence its acoustical performance (see Chapter 4).

Chapter 5 concerns the sound radiation of the structure using a simple approach (Rayleigh integral): infinite baffle plane radiator as a sum of point sources. The basis of this approach is shown in Section 1.2 and the results of the sound radiation of the wooden floor are presented.

1.1 Waveguide Finite Element Method

To carry out the vibrational analysis, a numerical approach based on WFEM is used. The method is suitable, in the frequency range from 0 to 200Hz, for systems with constant physical properties along, at least, one of its dimensions that will be referred as “waveguide” in this thesis.

WFEM uses a 2-D FE model over the cross-section of the waveguide and the Fourier transform along the waveguide to describe the vibrations of the system as a set of waves. The method reduces the computational effort and time compared with standard 3-D FEM tools. Additionally, the different wave types are easy to identify and study by using WFEM.

The Wavenumber Domain Software for Solids and Fluids, WANDS 2.1 ®, has been used to solve the models. The authorship and ownership of the software is the University of Southampton, UK. The output solutions from WANDS 2.1 ® have been loaded into MATLAB ® in order to evaluate other solution methods as the modal approach or the sound radiation.

Aalami (1973)(4) was the first one to derive solid WFEM for structures with isotropic material properties. Both, solid elements and simplify elastic material constants (assuming isotropic properties) are used in this thesis to model the floors.

1.1.1 Fundamentals

Most of the derivations used in this section follow the ones used by Sabiniarz (2004)(5).

Figure 1 is an example of a floor assuming constant properties and geometry along the X-dimension. The approximate wave equation (the time dependency is omitted), describing waves along the waveguide, is:

$$\left(\mathbf{K}_4 \frac{\partial^4}{\partial X^4} + \mathbf{K}_2 \frac{\partial^2}{\partial X^2} + \mathbf{K}_1 \frac{\partial}{\partial X} + \mathbf{K}_0 - \omega^2 \mathbf{M} \right) \hat{\mathbf{V}}(X) = \hat{\mathbf{F}}(X) \quad (1)$$

\mathbf{K}_i global cross sectional stiffness matrices

\mathbf{M} global cross sectional mass matrix

$\hat{\mathbf{V}}(X)$ vector of nodal displacements

$\hat{\mathbf{F}}(X)$ external loads

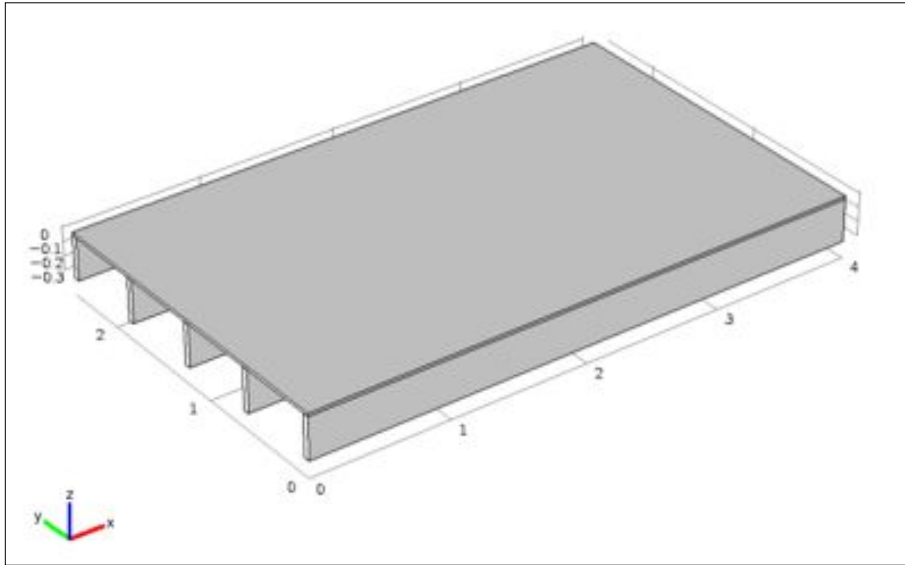


Figure 1 Structure with constant properties in the X-dimension.

In the absence of external load or source free form, solutions to the wave equation (1), representing waves travelling along the waveguide, are of the form:

$$\hat{\mathbf{V}}(X) = \mathbf{\Psi}e^{jkX} \quad (2)$$

$\mathbf{\Psi}$ cross sectional modeshape functions

k wavenumber

If these solutions are inserted into the homogeneous form of equation (1), we arrive to the next eigenvalue problem:

$$(\mathbf{K}_4k^4 - \mathbf{K}_2k^2 + \mathbf{K}_1jk + \mathbf{K}_0 - \omega^2\mathbf{M})\mathbf{\Psi} = 0 \quad (3)$$

There are two ways of solving the problem. We can find the modeshapes and wavenumbers for every selected frequency or we can solve the problem fixing the wavenumbers and getting the modal eigenfunctions and the eigenfrequencies. When the wavenumbers fulfill equation (4) and are inserted into equation (3) the eigenfunctions $(\Psi_{n,m})^1$ and eigenvalues $(\omega_{n,m}^2)^1$ are calculated for a finite floor with length "L".

$$k_n = \frac{n\pi}{L}, \quad (4)$$

$$n = \pm 1, \pm 2, \dots$$

L, length of the waveguide [m]

¹ "m" stands for the number of degrees of freedom (DoF) of the system

These calculations allow for analyzing the different types of waves, the cross sectional vibration pattern and the dispersion diagrams (k_n vs. $\omega_{n,m}$), among other parameters.

Additionally, to calculate the force response the modal approach is used (see equation (5)).

$$\hat{V}(X) = \sum_{n,m} \frac{\Psi_{n,m}^H \hat{S}}{[(1 - j\eta)\omega_{n,m}^2 - \omega^2] 2m_{n,m}L} \Psi_{n,m} (e^{-jk_n X} - e^{jk_n X}) \quad (5)$$

$\hat{V}(X)$ displacement field of a point excitation

$\hat{F}(X) = \hat{S}\delta(X)$ point force

η proportional damping of the whole system

$m_{n,m}$ modal mass (real scalar)

The exponential terms of equation (5) represent the propagating waves in each direction of the waveguide from the excitation point. These terms introduce the simply supported boundary condition in the system, i.e. every node of the cross section geometry is simply supported at the boundaries of the waveguide. The approach assumes that the different parts of the structure have the same damping (η). It is important to notice that to have reliable results over the frequencies of interest, modes of a wider frequency range must be summed up.

1.1.2 Methodology

MATLAB[®] has been used to generate the 2-D FE geometry (Y and Z-dimensions). The models are built with quadrilateral solid finite elements, each element with eight nodes. WANDS 2.1[®] uses a quadratic interpolation within the elements. Figure 2 shows an example of cross-section FE geometry highlighting one finite element. Each dot in the next figure represents a node and the corresponding nodal line in the waveguide (see Figure 3).

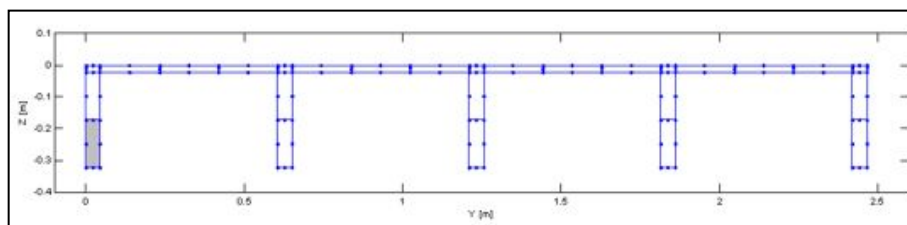


Figure 2 2-D FE geometry (Y and Z-dimensions) with highlighted finite element

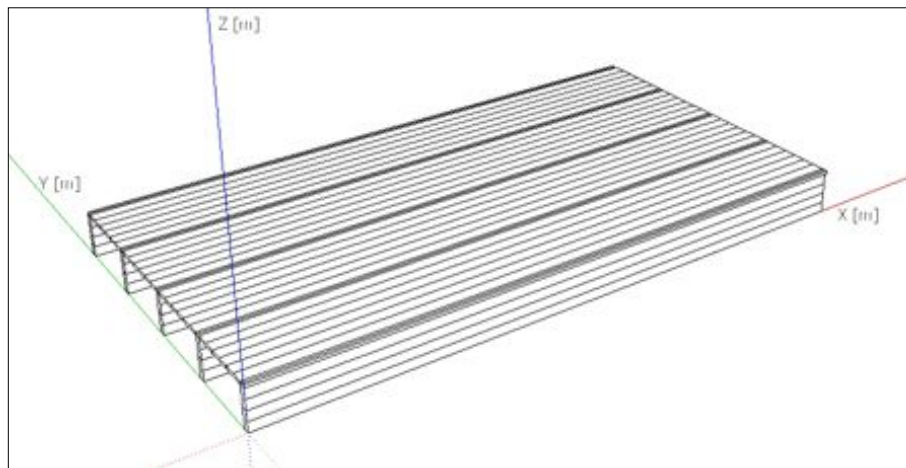


Figure 3 Detail of the nodal lines along the waveguide (X-dimension)

The number of elements for each modelled structure depends on the geometry and the upper frequency limit of interest. As rule of thumb, at least six elements per wavelength are needed in order to reproduce the vibrational behaviour with sufficient accuracy and within a reasonable computational effort. A preliminary study was done to evaluate the influence of the number of elements; the results are given in Chapter 2.

Regarding the elastic material properties of the structure, all the elements have been considered made of an isotropic material. Even when it was considered a dramatic simplification not to define wood as an orthotropic material, the assumption was accepted for simplicity. Which it is important for and for the understanding of the performance of the LWF. The elastic parameters used in the models are: Young's modulus (E [N/m²]), Poisson's ratio ([-]), Density ([kg/m³]) and Loss Factor ([-]).

Apart from the boundary conditions introduced in the waveguide by using equation (5), WFEM allows to constraint the displacement (u_x , u_y and/or u_z) of any node of the cross-section geometry.

The solutions from WANDS 2.1 ® are the global cross sectional complex stiffness (K_i) and mass (M) matrices. Those matrices are used in MATLAB ® for the calculations of the dispersion diagrams, structure deformations, mobilities, etc.

1.2 Sound radiation

Once the spatial distribution and the amplitude of the vibrations of the floor are known, it is possible to predict the sound radiation in the frequency range of interest. No fluid loading is taken into account during the calculations.

The main parameters to be calculated are the radiated sound power (W) and the associated sound power level (L_w). We have used the "Plane, baffle radiator" approach to carry out the calculations (the method can be found in Section 7.5 Cremer, Helckl and Petersson (2005)(6)). This approach is based on assuming a baffle plane radiator (top board of the LWF) as a sum of point sources which can be considered as monopoles in a large baffle (see Figure 4). Each point source radiates the volume velocity that is calculated as:

$$q_0 = v_0 S \quad (6)$$

q_0 , volume velocity [m^3/s]

v_0 , amplitude of the velocity field [m/s]

S , section area of the point source [m^2]

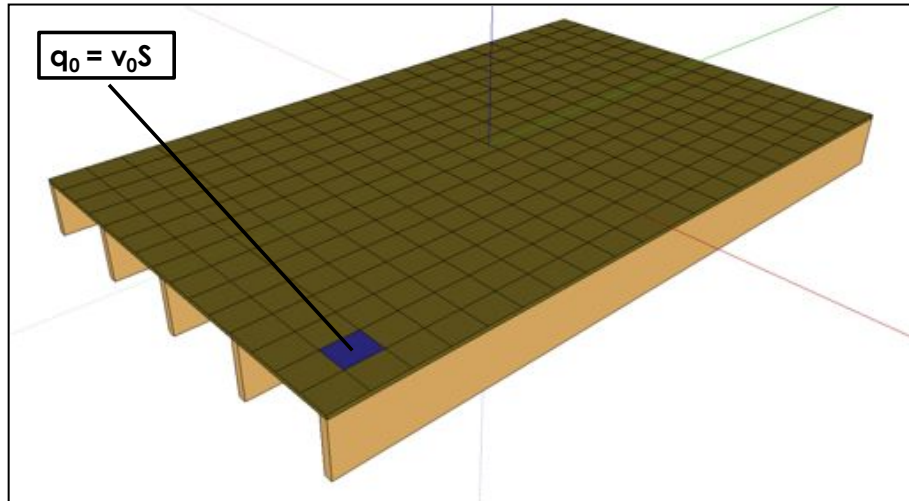


Figure 4 Floor's mesh. Plane baffle radiators as point sources

Once the volume velocity for each point source of the floor's top board has been calculated, the contribution of each source to the total sound pressure at any point at a certain distance from the sources is just the simple summation given in Equation (7) which dates from Lord Rayleigh:

$$p = \frac{j\omega\rho_0}{2\pi} \left[\frac{q_1}{r_1} e^{-jk_0 r_1} + \frac{q_2}{r_2} e^{-jk_0 r_2} + \dots \right] = \frac{j\omega\rho_0}{2\pi} \left[\sum_{n=1}^N \frac{q_n}{r_n} e^{-jk_0 r_n} \right] \quad (7)$$

p , sound pressure [Pa]

ω , angular frequency [rad/s]

ρ_0 , density of fluid (air) [kg/m^3]

q_n , volume velocity at point source "n" [m^3/s]

r_n , distance from point source "n" to the receiving point [m]

k_0 , wavenumber in the fluid (air) [rad/m]

If instead of calculating the sound pressure for just one point, we place "m" receiving points² over the surface area of a hemisphere surrounding the structure in free field conditions, the radiated sound power can be calculated. The origin of the hemisphere has been chosen at the centre of the structure

² Each receiving point corresponds to an equal surface area of a hemisphere surrounding the floor in free field conditions.

and the sound pressure is calculated for each of the receiving points (p_i). The radiated sound power is calculated as:

$$W = \frac{\pi R^2}{\rho c} \frac{1}{m} \sum_{i=1}^m |p_i|^2 \quad (8)$$

W , radiated sound power [W]

R , radius of the hemisphere [m]

ρ_0 , density of the medium [kg/m^3]

c_0 , wave speed of the medium [m/s]

m , is the total number of receiving points

p_i , sound pressure at receiving position "i" [Pa]

From this the radiated sound power level from the structure can be calculated using:

$$L_W = 10 \log \left(\frac{W}{W_0} \right) \quad (9)$$

L_W , radiated sound power level [dB re. 1 pW]

W_0 , reference power [1 pW]

The radiated sound power can be also related to the averaged velocity on the floor. This is expressed as the radiation efficiency " σ ":

$$\sigma = \frac{W}{\rho_0 c_0 S \overline{|v|^2} / 2} \quad (10)$$

W , sound power [W]

ρ_0 , density of the medium [kg/m^3]

c_0 , wave speed of the medium [m/s]

S , floor surface [m^2]

$\overline{|v|^2}$, spatially averaged mean square velocity of the structure [m^2/s^2]

2 Models

This chapter presents the main features and parameters used in the design of the models, including an analysis of the influence of the number of finite elements. The last two sections present the analysis of the wave field and mobilities comparing the results of both modelled floors.

The analyzed structures are very simple: the lightweight floor consists on a top board lying on five beams while the heavyweight floor is just a concrete plate. The dimensions of both structures (see *Table 1*) and the way the FE geometries have been designed make the results comparable between them.

Table 1 Dimensions of the floors

Reference direction	Dimension [m]
X	4.0
Y	2.465
Z	0.3

2.1 Finite Element resolution

The number of finite elements used when building a FE model is of main influence in the final results. If not enough elements are used the structure appears “stiffer”, therefore, the results are erroneous. The number of elements is related with the highest frequency to be analyzed; at least six elements per wavelength are recommended to obtain results within a reasonable precision. On the other hand, the more elements used the more computational effort and time is consumed. Therefore, it is needed to find a compromise between computational effort and accuracy.

Two models of the HWF and another two for the LWF have been built using low and high element resolution scenarios. Figure 5, Figure 6, Figure 7 and Figure 8 show their cross-section geometries and *Table 2* gives the number of finite elements used in each of them.

Table 2 Number of finite elements used in each model

Structure	Low resolution FE	High resolution FE
HWF	34	225
LWF	27	65

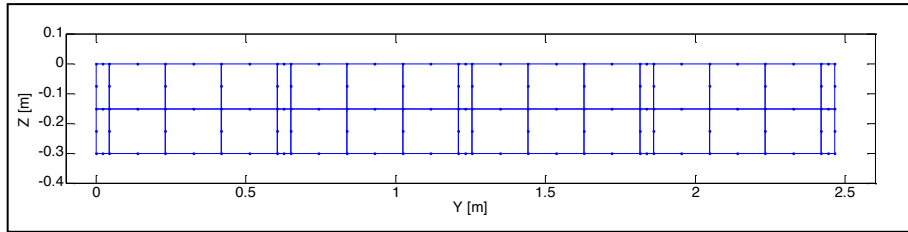


Figure 5 HWF 2-D FE geometry (low element resolution)

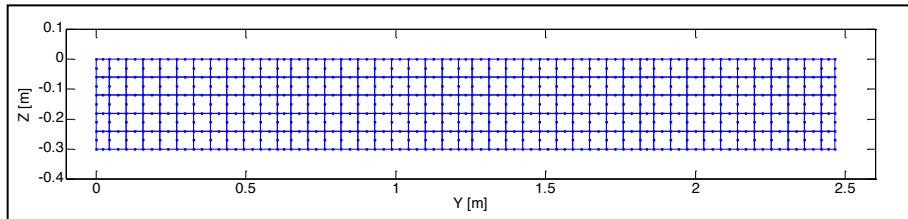


Figure 6 HWF 2-D FE geometry (high element resolution)

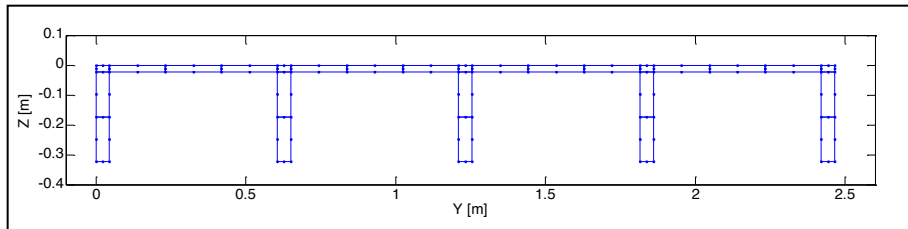


Figure 7 LWF 2-D FE geometry (low element resolution)

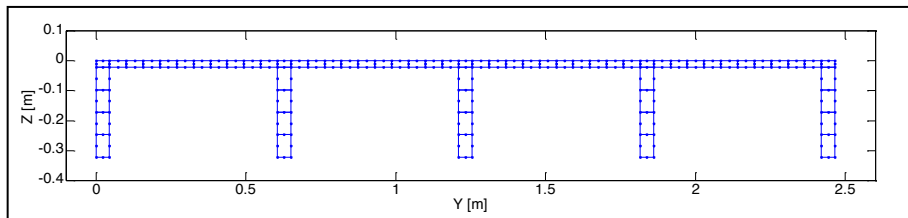


Figure 8 LWF 2-D FE geometry (high element resolution)

The point mobility, at one point on top of the structures, is presented in Figure 9 and Figure 10 for HWF and LWF respectively. During the analysis of the results, we have differentiated between frequency and level changes at the resonances.

From the level point of view, the more elements used the more damped is the system. Relative to the frequencies at the resonances, the graphs are showing how, for the HWF, there is not significant change between both resolutions and thus the low resolution model will be used in the rest of the work. However, for the LWF the change is noticeable enough and therefore the high resolution model will be used from now on.

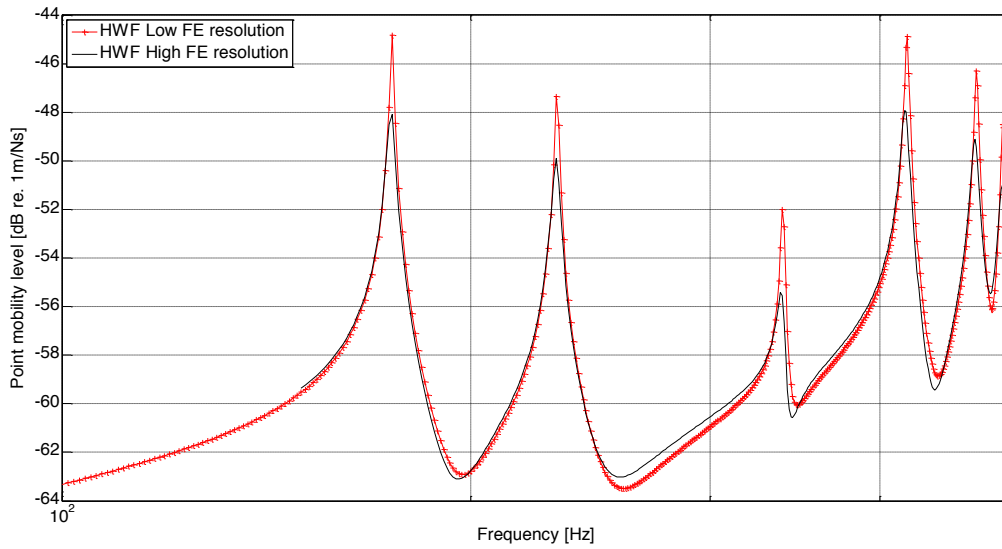


Figure 9 HWF FE resolution comparison

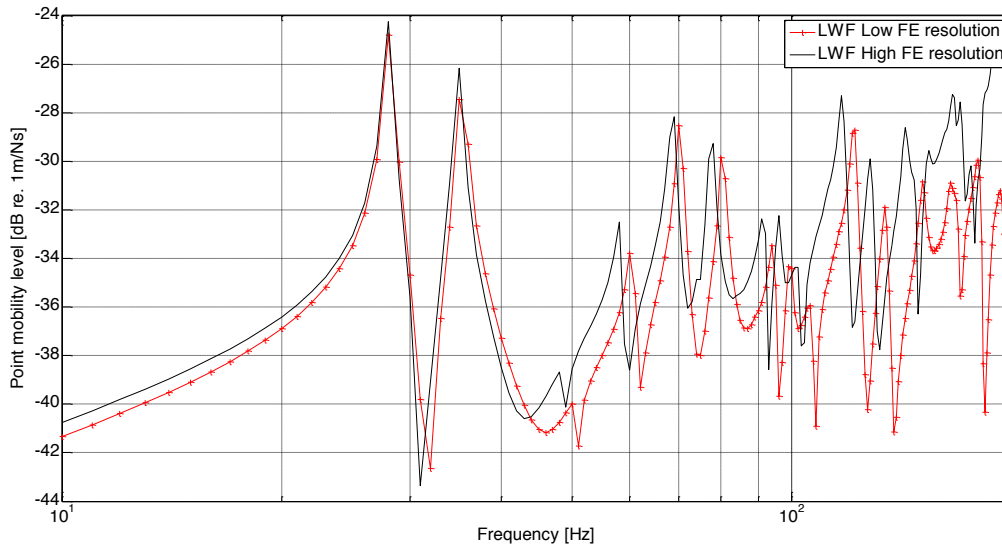


Figure 10 LWF FE resolution comparison

2.2 Heavyweight floor (HWF)

The model represents a simple concrete floor (see Figure 11). The main data of the 2-D FE model are given in the *Table 3* and the geometry is shown in Figure 12 together with the restrained nodes. The boundary conditions consisted on constraining all the DoF (u_x , u_y and u_z displacements) of the indicated nodes. Finally, the material data and its elastic properties are given in *Table 4*.

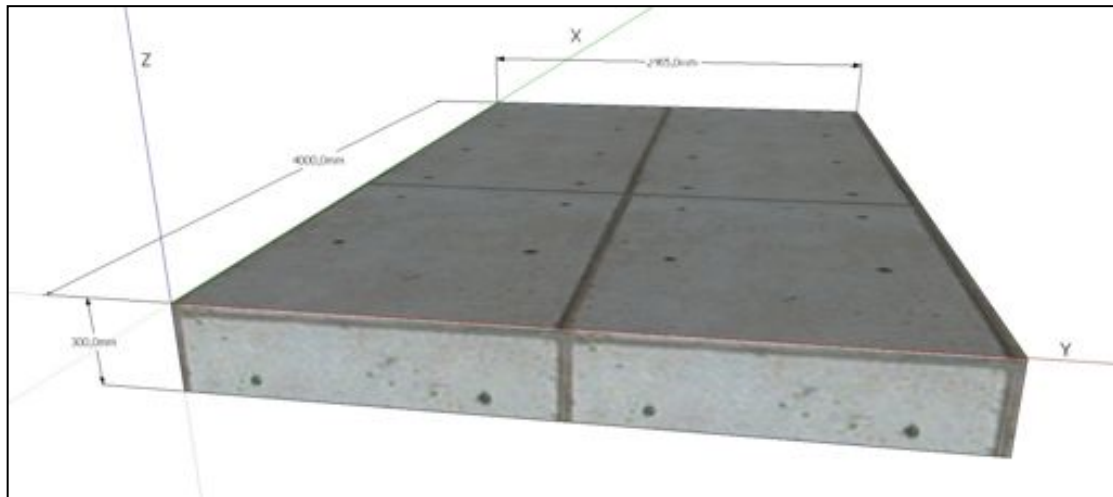


Figure 11 Detail of the HWF

Table 3 FE model data of the HWF

Elements	34
Nodes	141
DoF	393
Restrained nodes	10
Restrained displacements	u_x u_y u_z

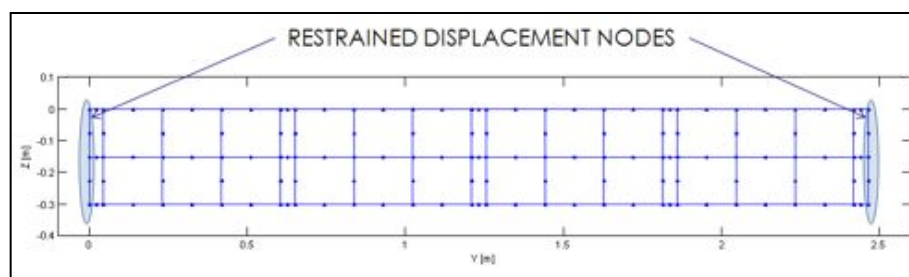


Figure 12 2-D FE geometry of the HWF and boundary conditions

Table 4 Material data of the HWF

Material data	HWF
Material	Concrete
Type	Isotropic
Young's modulus [N/m ²]	26 10 ⁹
Poisson's ratio [--]	0.2
Density [kg/m ³]	2300
Loss factor [--]	6 10 ⁻³

2.3 Lightweight floor (LWF)

The modelled lightweight structure is the simple wooden floor shown in Figure 13. The top board is made of "Chipboard" and the beams are built with "KERTO ®". Table 5 includes the data of the FE geometry and boundary conditions (see Figure 14). Table 6 includes the information related with the floor materials. As before, the boundary conditions consist of restraining the u_x , u_y and u_z displacements of the indicated nodes.



Figure 13 Detail of the LWF

Table 5 FE model data of the LWF

Elements	65
Nodes	328
DoF	918

Restrained nodes	22
Restrained displacements	$u_x u_y u_z$

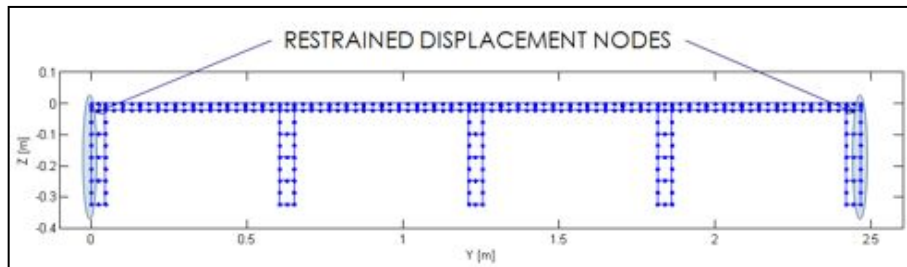


Figure 14 2-D FE geometry of the LWF and boundary conditions

Table 6 Material data of the LWF

Material data	LWF - Board	LWF - Beams
Material	Chipboard	Kerto
Type	Isotropic	Isotropic
Young's modulus [N/m^2]	$3.4 \cdot 10^9$	$4.4 \cdot 10^9$
Poisson's ratio [--]	0.4	0.4
Density [kg/m^3]	710	560
Loss factor [--]	0.03	0.01
Proportional loss factor (for mobility calculations)	0.02	

2.4 Wave field analysis

One of the main benefits of using WFEM, is the fact that the vibrations are described as waves along the waveguide. These waves can be identified and analyzed independently from each other, giving a deeper physical understanding of the investigated structure.

2.4.1 Interpretation of the dispersion diagrams

One of the most important tools to analyze the wave field on the structure is the so called “Dispersion” diagrams, which is a representation of how the wavenumbers are related to the frequency for each propagating wave along the structure.

A vector of wavenumbers values (k_i) is introduced in the calculation process and the eigenproblem is solved for the corresponding eigenfrequencies ($\omega_{k_i,m}$) and eigenfunctions ($\Psi_{k_i,m}$). If the wavenumbers (k_i) take any value, the eigenproblem is solved assuming an infinite waveguide. This is shown in Figure 15 and Figure 16 for HWF and LWF respectively, where the vector takes values from 0 to 10 with a resolution of 0.01. When the wavenumbers (k_i) fulfil the condition given in Equation (4), then the solutions are calculated for a finite waveguide. Figure 17 and Figure 18 show the dispersion diagrams for the floors with a finite length (L).

The dispersion diagrams together with the deformation plots allow to classify the waves as “Bending Waves” (BW) or “Longitudinal Waves” (LW). This classification has not been straightforward, at least for the LWF, since the dispersion diagrams represent discrete results and not continuous lines (even that they have the appearance of lines when the wavenumber resolution is high enough) and the different waves frequently intersect each other. The results of the classification are shown in Figure 17 and Figure 18. The figures show at least the first six bending waves of both floors. These waves will be the main responsible of the sound radiation in the frequency range of interest.

The numbering of the bending waves (BW01, BW02, etc.) is related with the eigenfunctions or modal shapes order. When the floor is a simple plate as the HWF, it is easy to understand why the modal shapes are connected to represent a wave but for more clarity *Table 7* to *Table 12* include those cross-section deformations for the first six bending waves.

Figure 17 and Figure 18 show how to have the first six bending waves in the concrete floor we have to go up to 2 kHz, while for the wooden floor we just need to go up to 100 Hz. Appendix A includes a table with the values of the eigenfrequencies for the finite length floors.

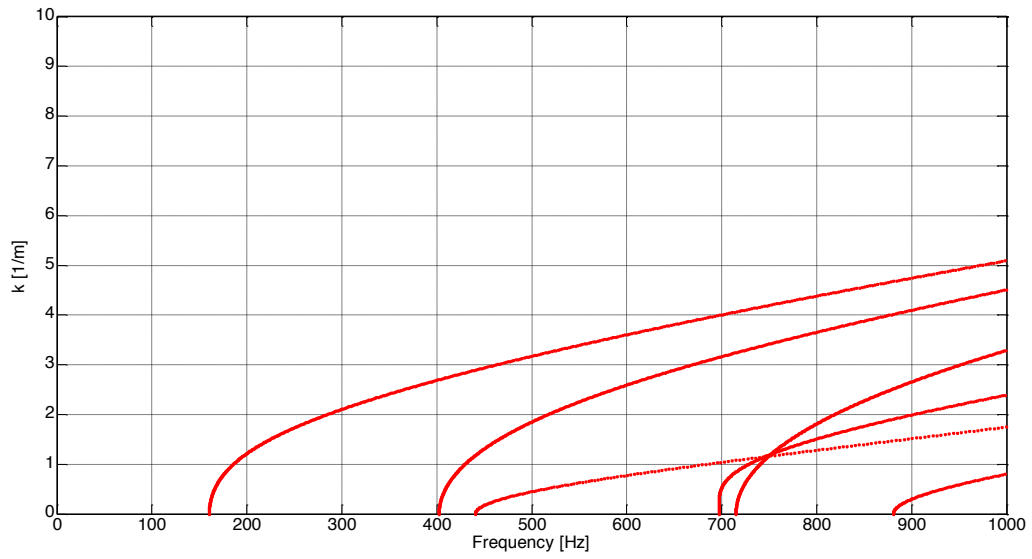


Figure 15 Dispersion diagram of the HWF

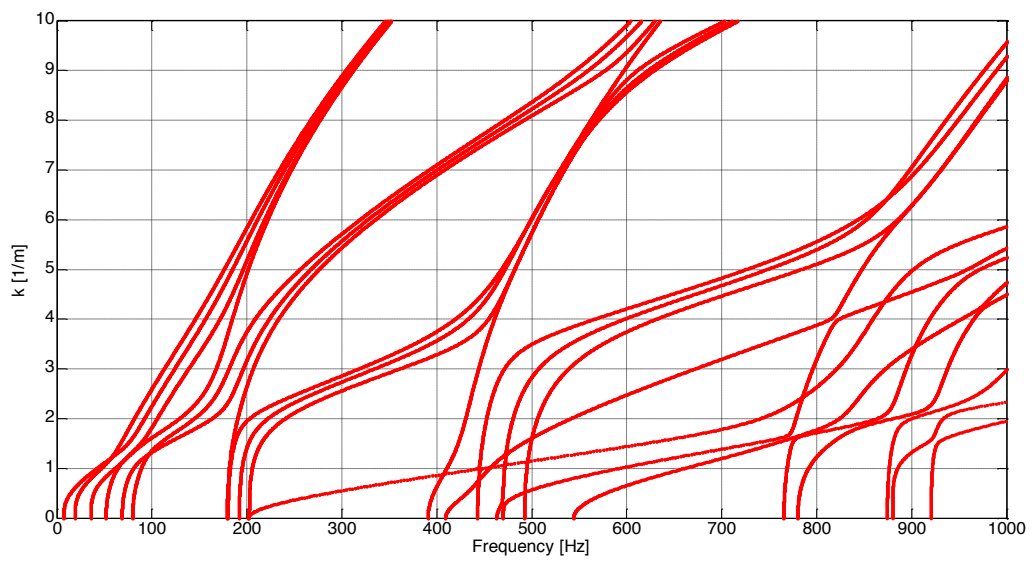


Figure 16 Dispersion diagram of the LWF

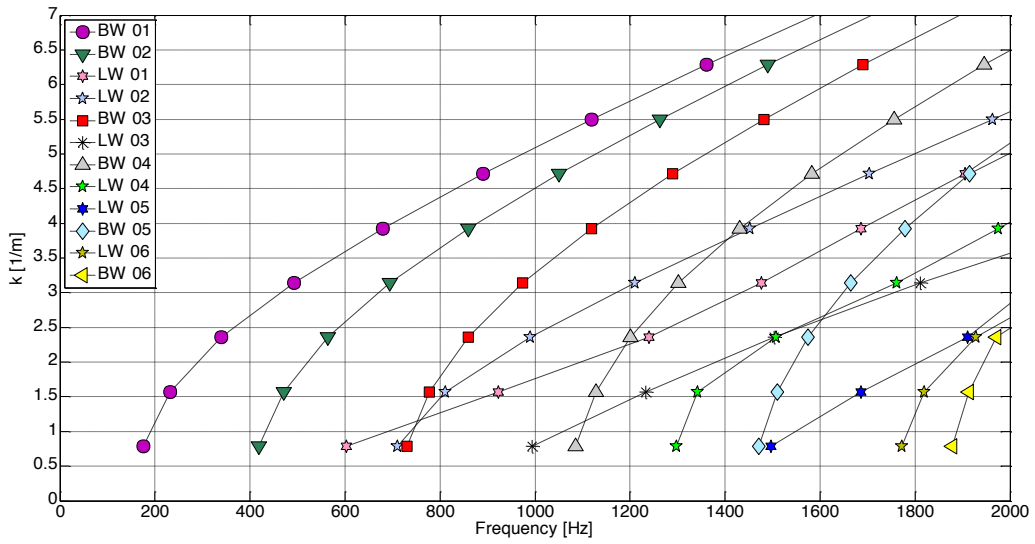


Figure 17 Waves classification for the HWF

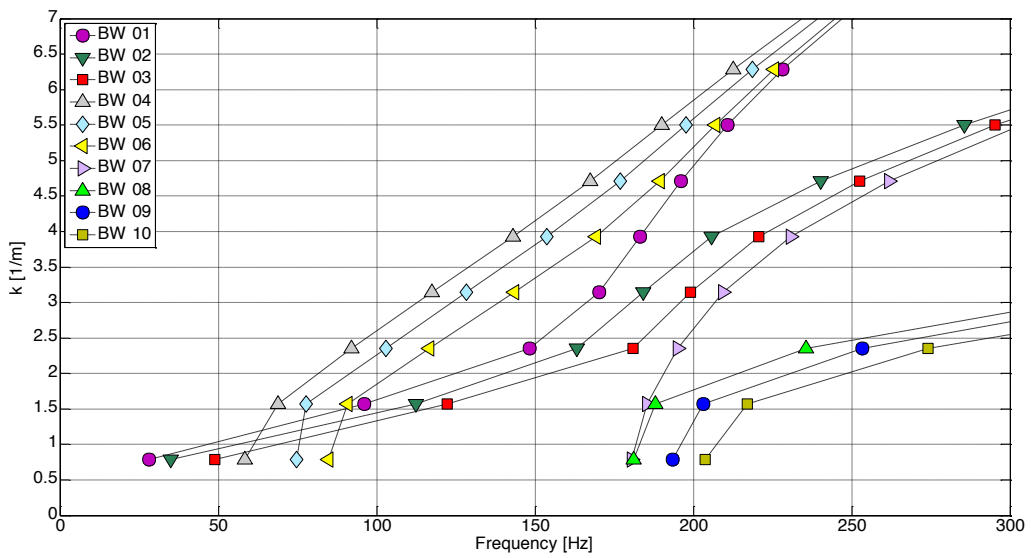


Figure 18 Waves classification for the LWF

2.4.2 Analysis of the deformation diagrams

Another tool to analyze the wave field is to plot the deformations of the floors. We can easily compare the 2-D cross-section deformations (a certain transversal “cut” of the floor) or the top layer deformation.

As before, we focus our analysis in the six lowest order free bending waves (see Figure 17 and Figure 18), plotting the deformations of both floors only for the first four modal wavenumbers ($k_n, n=1,2,3,4$).

The results presented in *Table 7* to *Table 12* show clearly how the influence of the beams in the vibrations of the LWF become noticeable from the second modal wavenumber and higher order modes. The deformations of the HWF are those of a simple plate where the different modes can be easily identified. Another conclusion from the deformation plots is how the first order mode ($k_n, n=1$) of the LWF is similar to that of the HWF. For increased clarity, the LWF is vibrating as a simple plate for the first order modes and lowest order waves.

Table 7 Deformation plots BW01

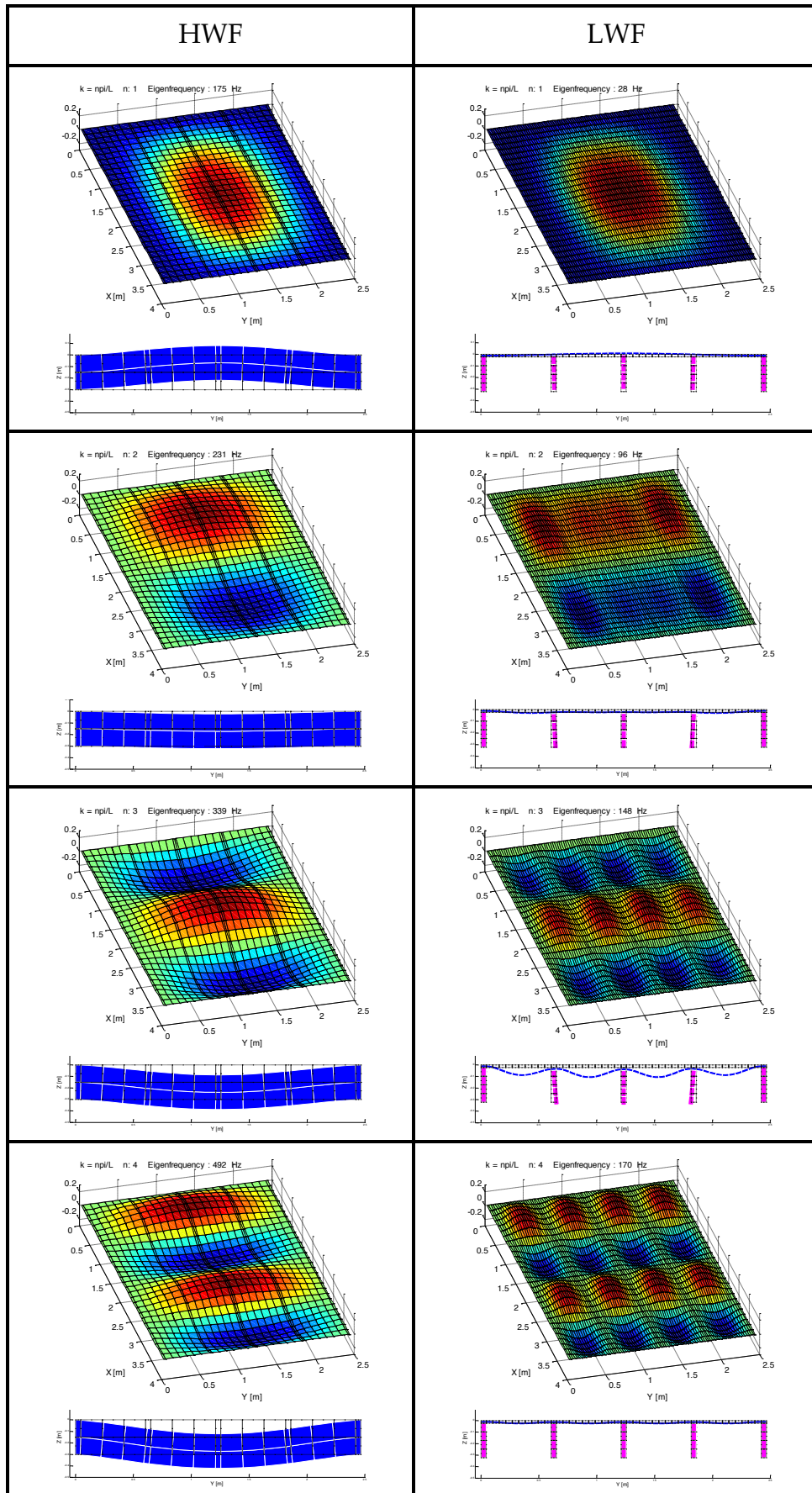


Table 8 Deformation plots BW02

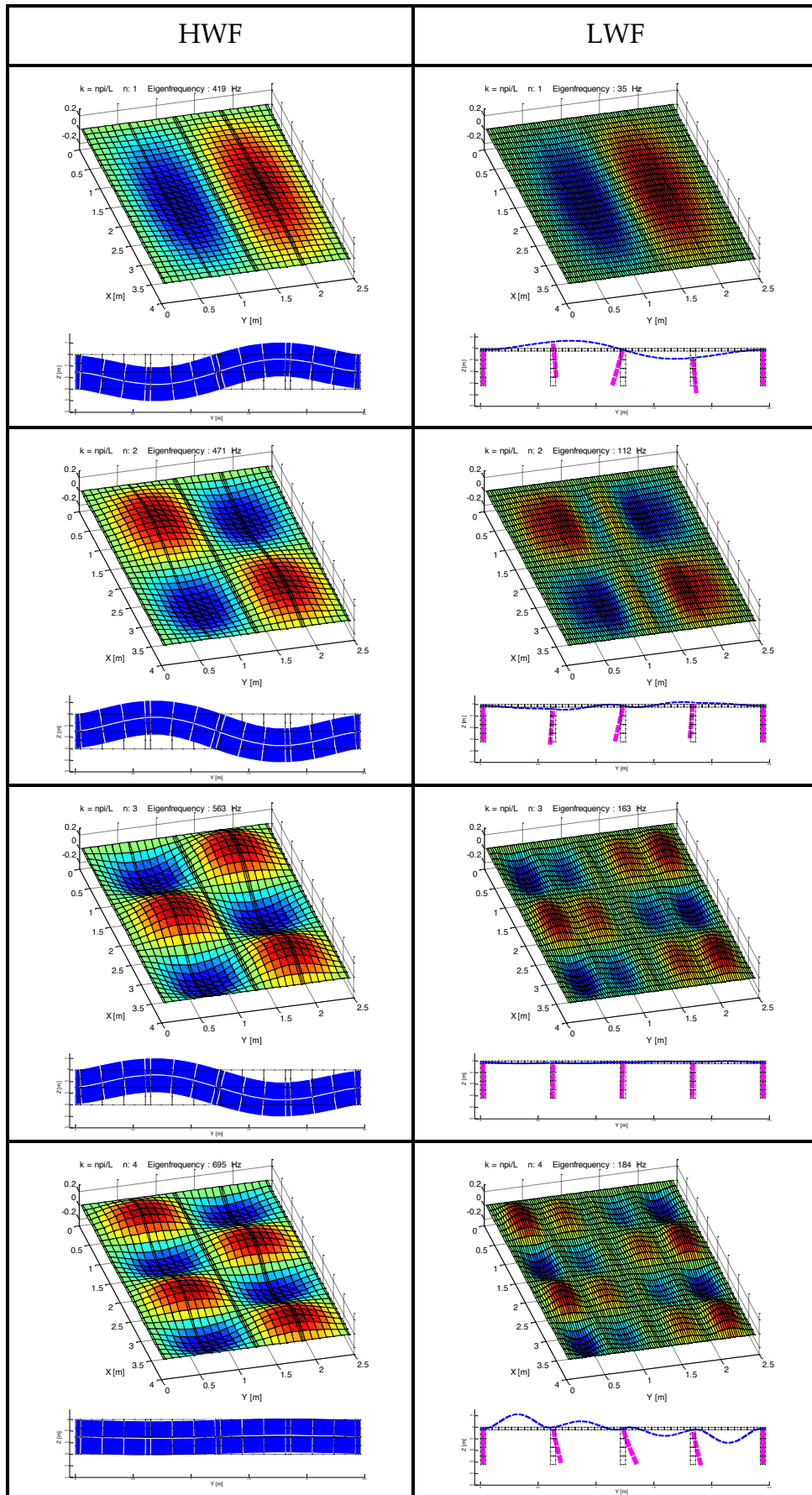


Table 9 Deformation plots BW03

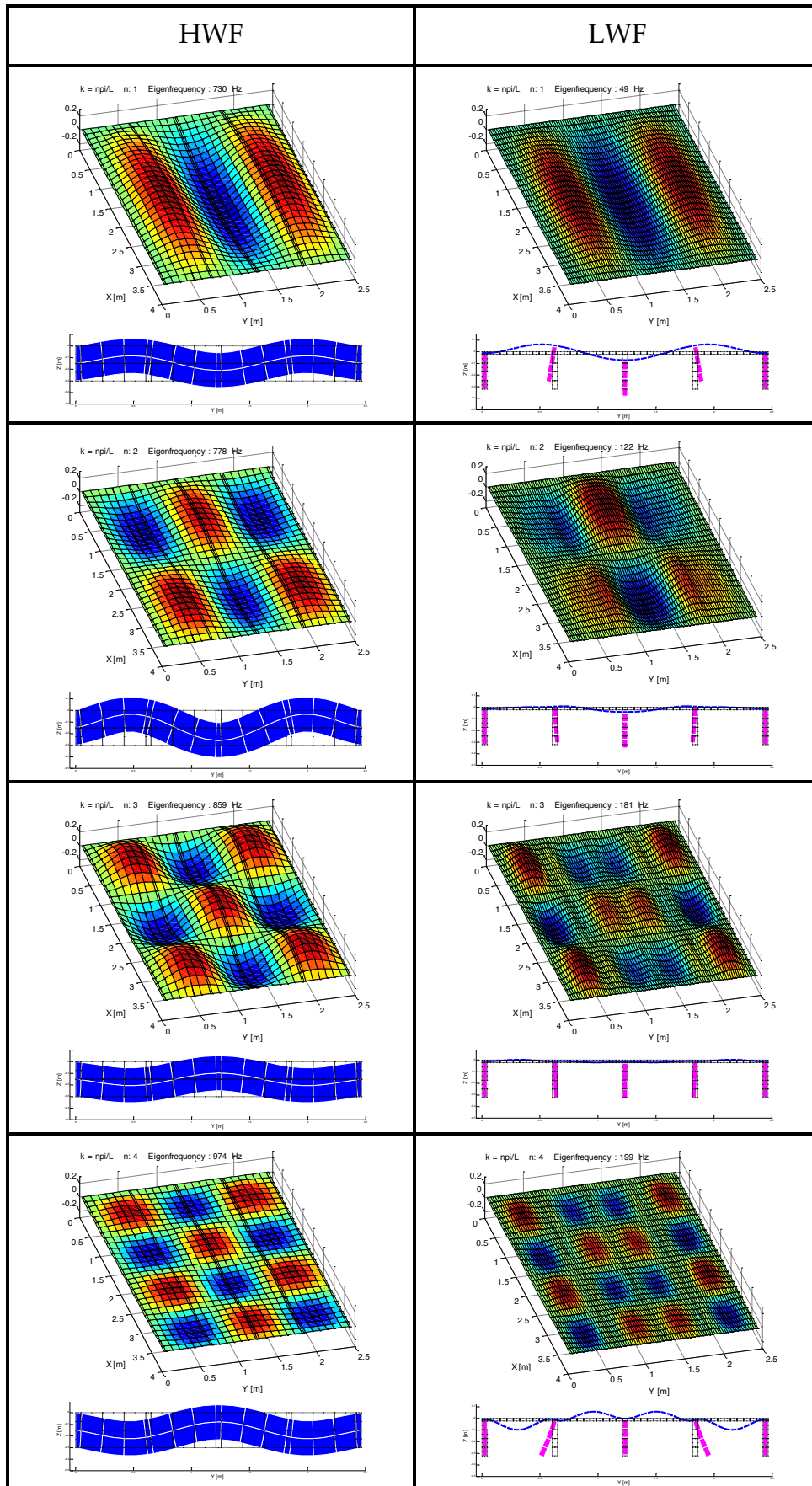


Table 10 Deformation plots BW04

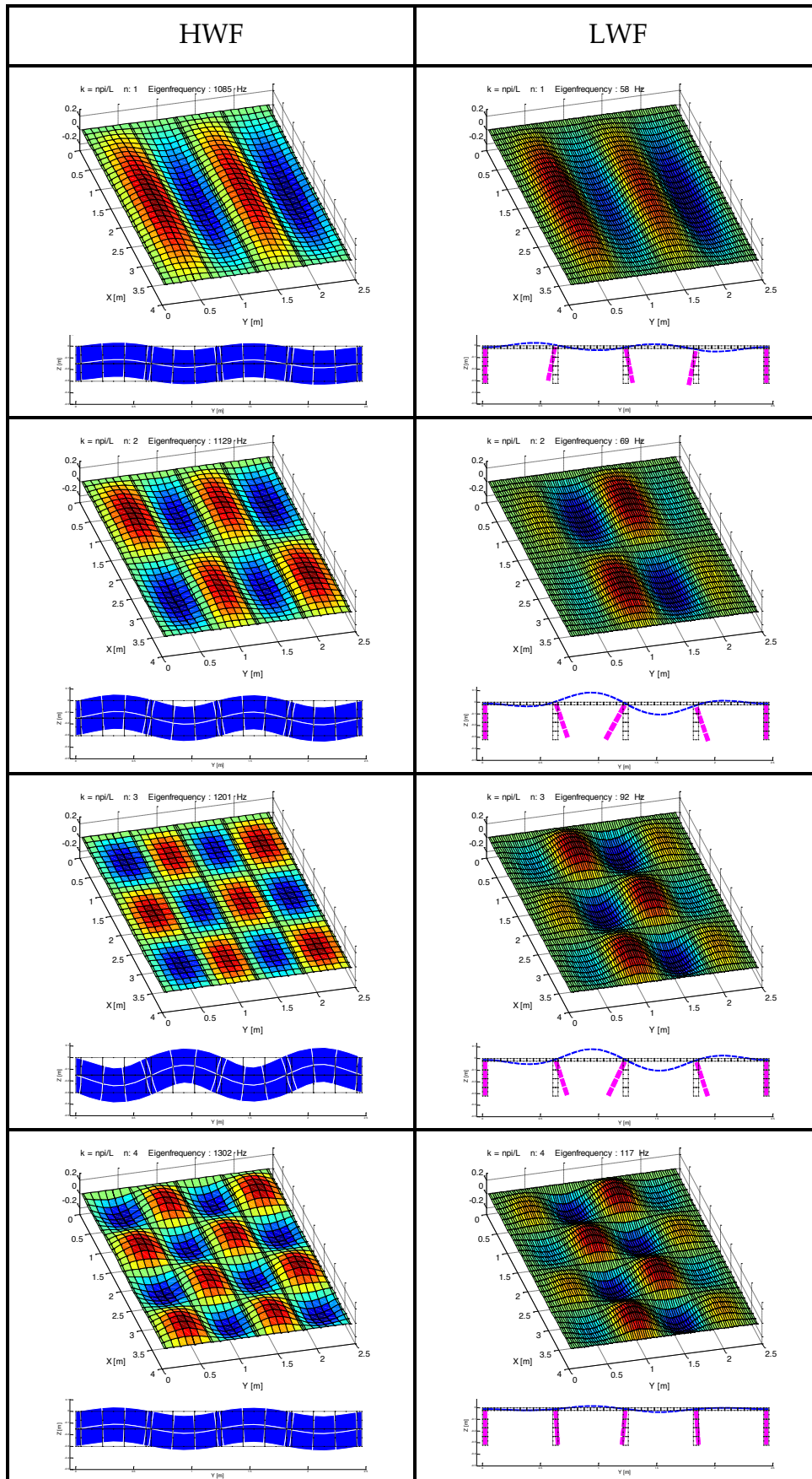


Table 11 Deformation plots BW05

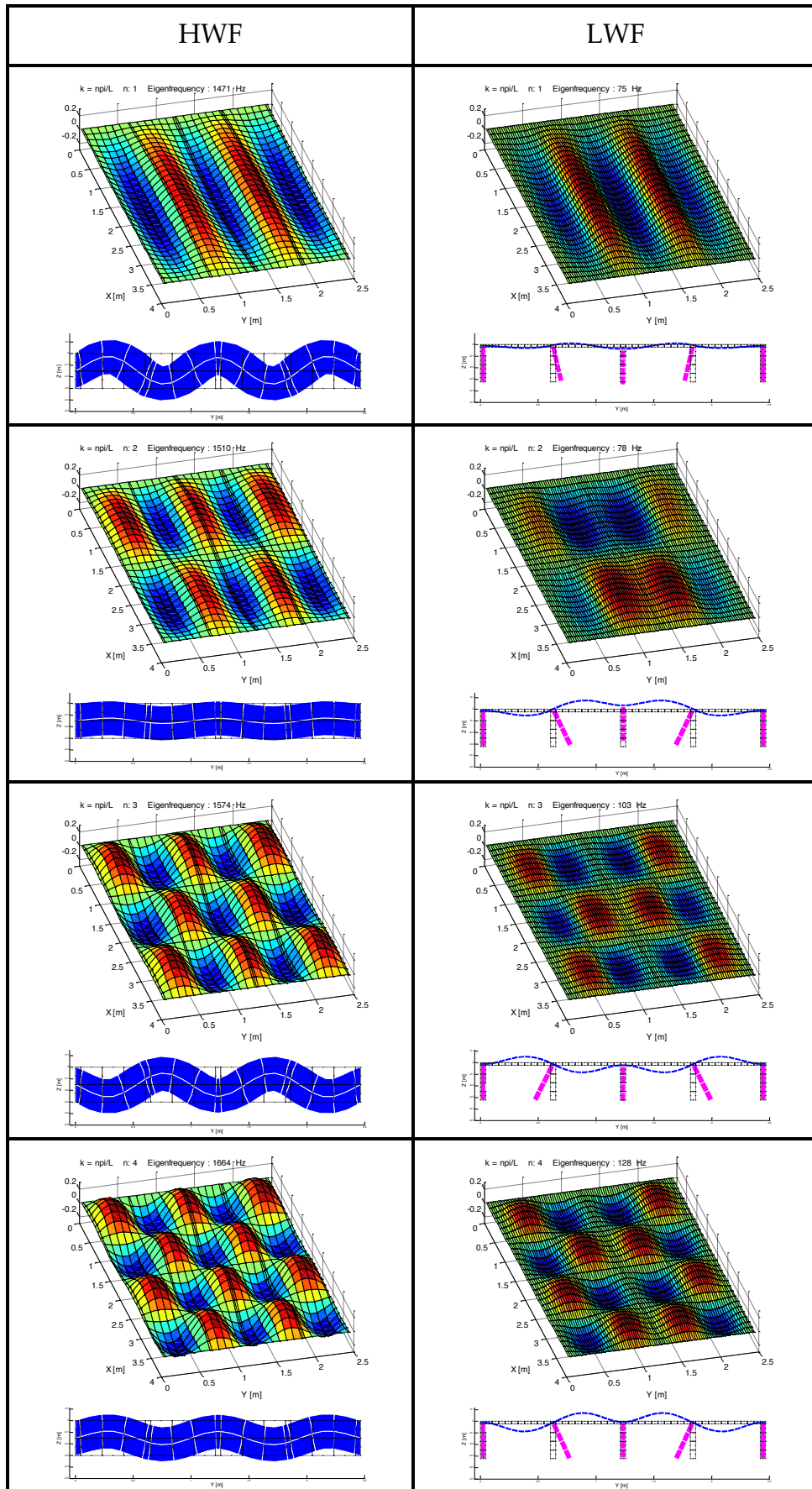
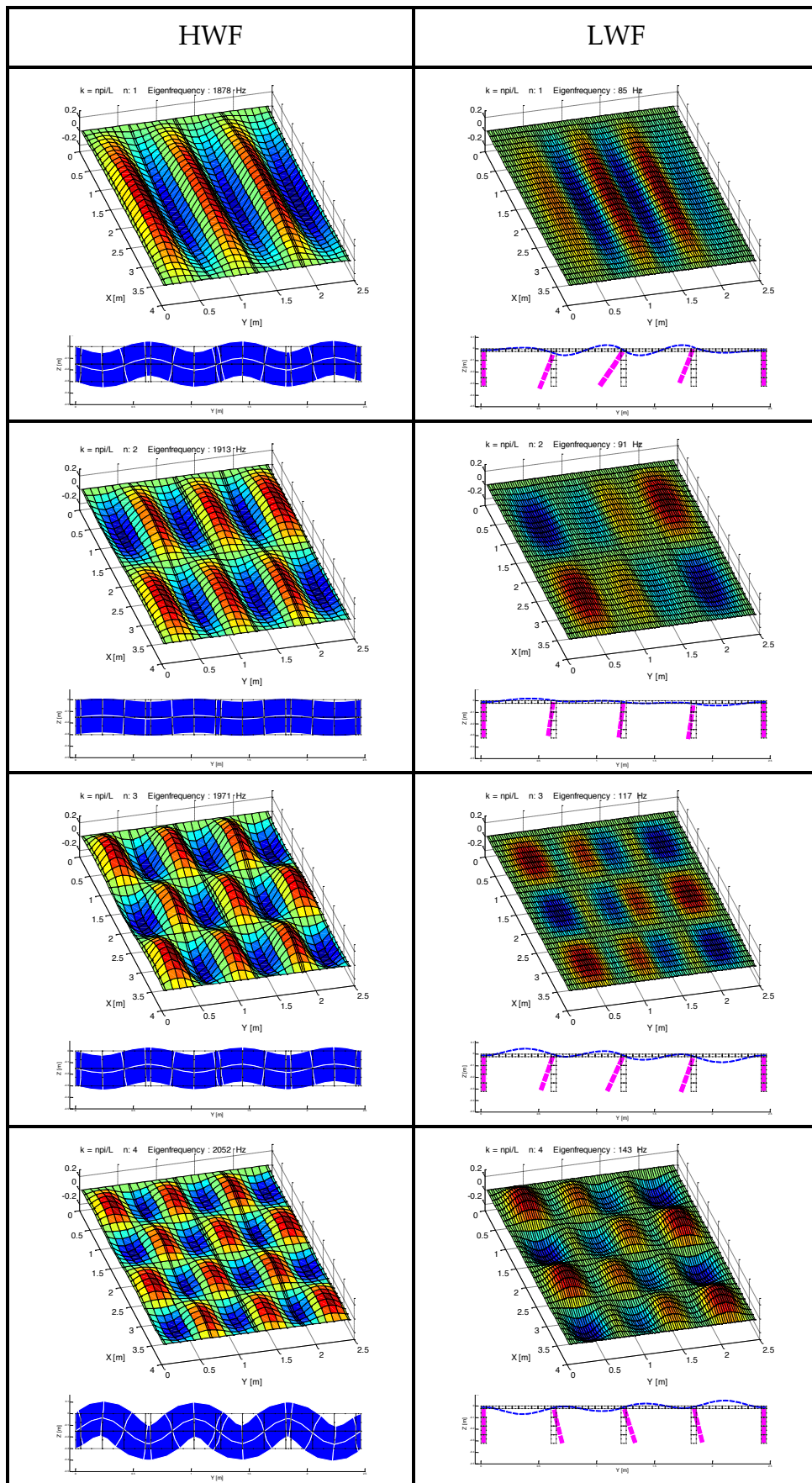


Table 12 Deformation plots BW06



2.5 Mobility analysis

As we indicated in Section 1.1.1, the force response of the structures can be calculated using Equation (5). This method allows introducing a force at any point situated on a nodal line at any distance from the boundary of the waveguide. Once the force has been applied, the point mobility or the transfer point mobility at any point of the structure can be calculated. The last parameters left are the direction of the force and what DoF of the velocity field (v_x , v_y , v_z) is of interest at the reception point.

In our calculations, a unit point force has been defined normal to the Z-dimension of the floors. The points where the point mobility has been calculated are shown in Figure 19. They have been chosen to have one point on top of a beam (P1) and a second point between two beams (P2). Exactly the same points have been chosen in the concrete floor. The results are shown for the Z-direction of the velocity field.

This approach is valid as long as we assume uniform damping over the whole system and when all the modes over the frequency range of interest are summed up.

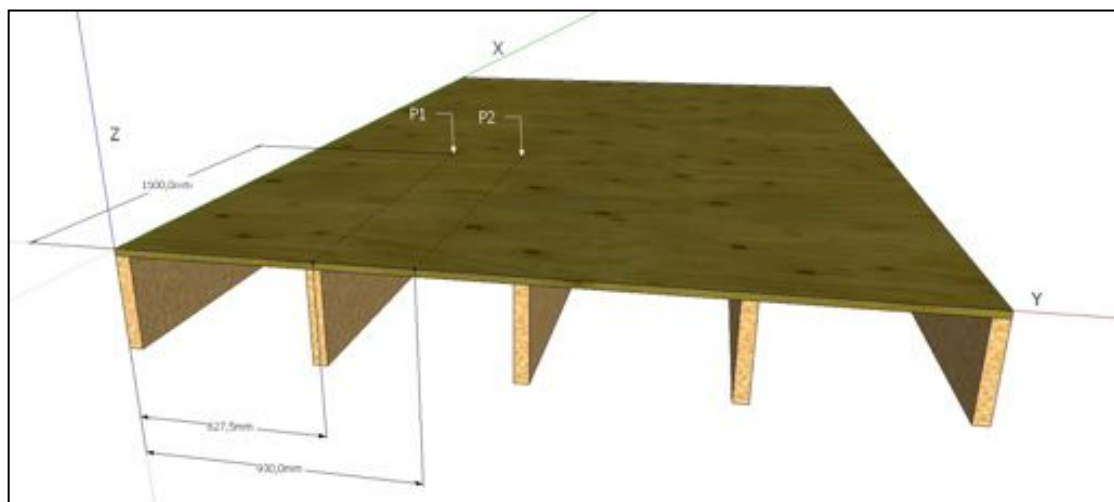


Figure 19 Position of the points used to calculate the point mobilities.

Figure 20 and Figure 21 show the point mobility at position P1 for the HWF and LWF, respectively. Again, it can be seen how the LWF vibrational field is much more complex than the HWF field in this frequency range. Furthermore, as expected, it is easier to put energy into the LWF than the HWF. Therefore, the mobility level at the resonances is normally smaller in the latter case.

The point mobilities of P1 and P2 for the LWF are compared in Figure 22. The mobility at point P2 (between beams) has normally a bigger level when the same resonance is excited at both points.

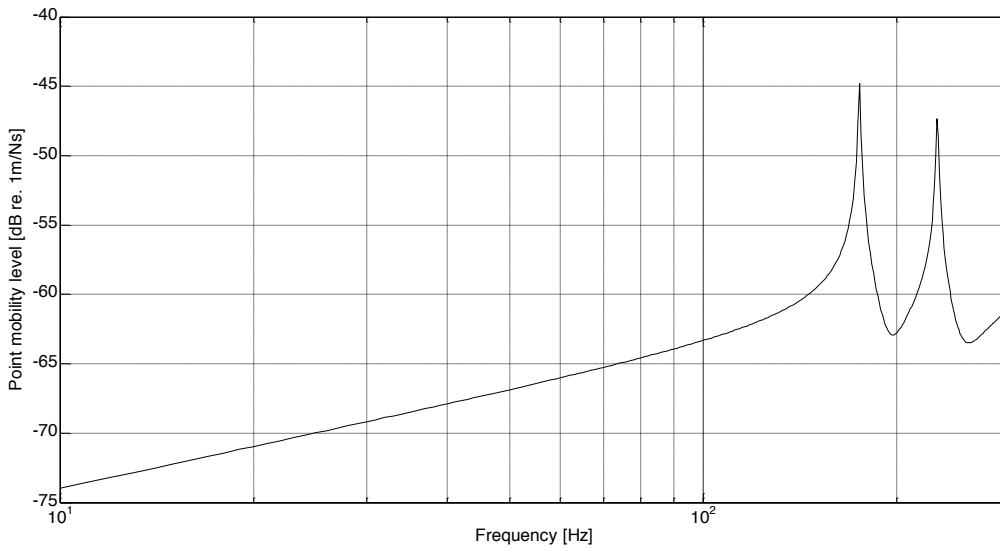


Figure 20 HWF point mobility at P1.

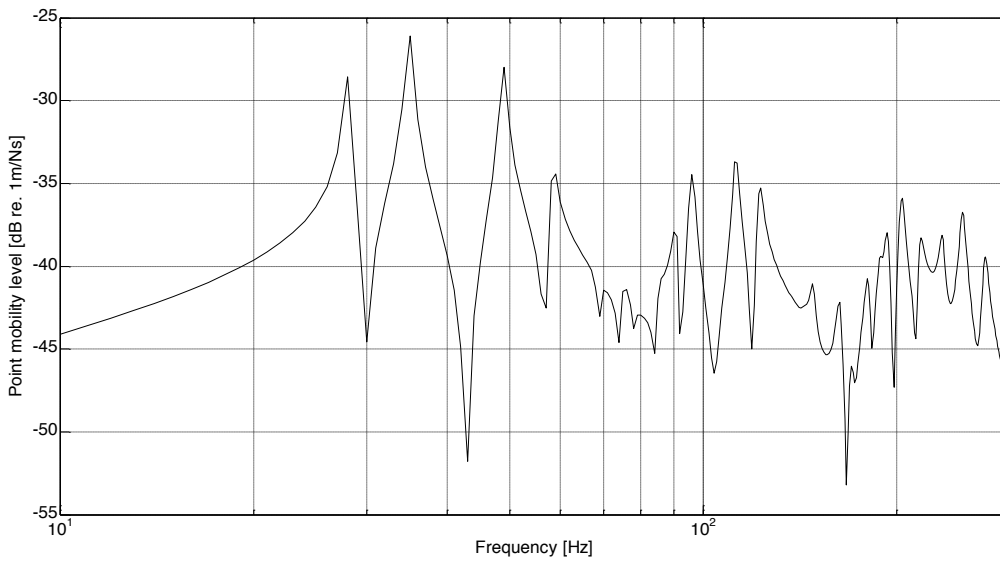


Figure 21 LWF point mobility at P1.

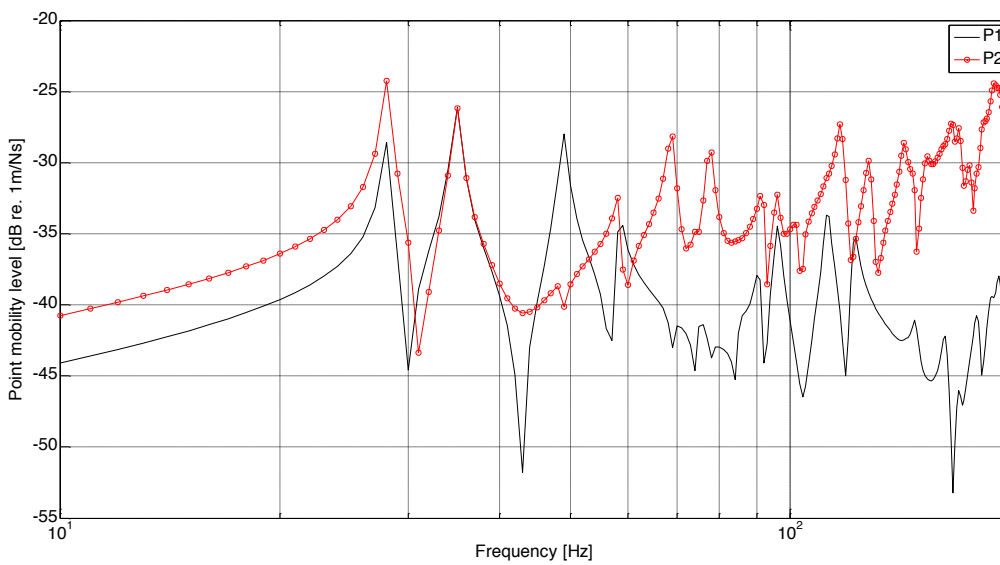


Figure 22 LWF point mobilities comparison (P1 – P2).

3 Validation

The results from WFEM have been compared with those of the same structure but modelled using normal FEM. The software used for the calculations has been COMSOL Multiphysics ®. The modelled structure has the same geometry, material properties and boundary conditions than the ones used for the LWF when using WFEM. Figure 23, Figure 24 and Figure 25 show some details of the meshed structure and the constraint elements (blue highlighted). The boundary conditions in the waveguide direction have been introduced by constraining the displacement of the board top edges. *Table 13* includes the main data of the FEM model:

Table 13 Main data of the FEM model

Elements type	Tetrahedral
Number of elements	14676
Mesh size	Coarse
DoF	89283
Solver	Spooles
Average element quality	0.5042

The point mobility is calculated at the same points P1 (on beam) and P2 (between beams) used in the WFEM calculations (see Figure 19).

Figure 26 and Figure 27 are showing the results for points P1 and P2 respectively. These graphs are showing the comparison between the calculated point mobilities using WFEM and FEM. *Table 14* is giving the frequency percentage deviations³ at the eigenfrequencies for the first six bending waves and lowest order modes. The frequency differences never get over 10% and the level deviations are below 3 dB (up to 150 Hz) what can be considered reasonable for the purposes of this work.

The differences between the deformation plots using WFEM and FEM for the lowest order modes are shown in Appendix B. It is important to highlight the differences of some deformation plots (p.e. BW02 for k_3 and BW03 for k_3) since WFEM uses a sine function to propagate the wave along the waveguide and this is not always the appropriate solution for the real situation.

³ FEM eigenfrequencies have been considered the reference values in the percentage calculations and have been calculated using “finer” mesh size.

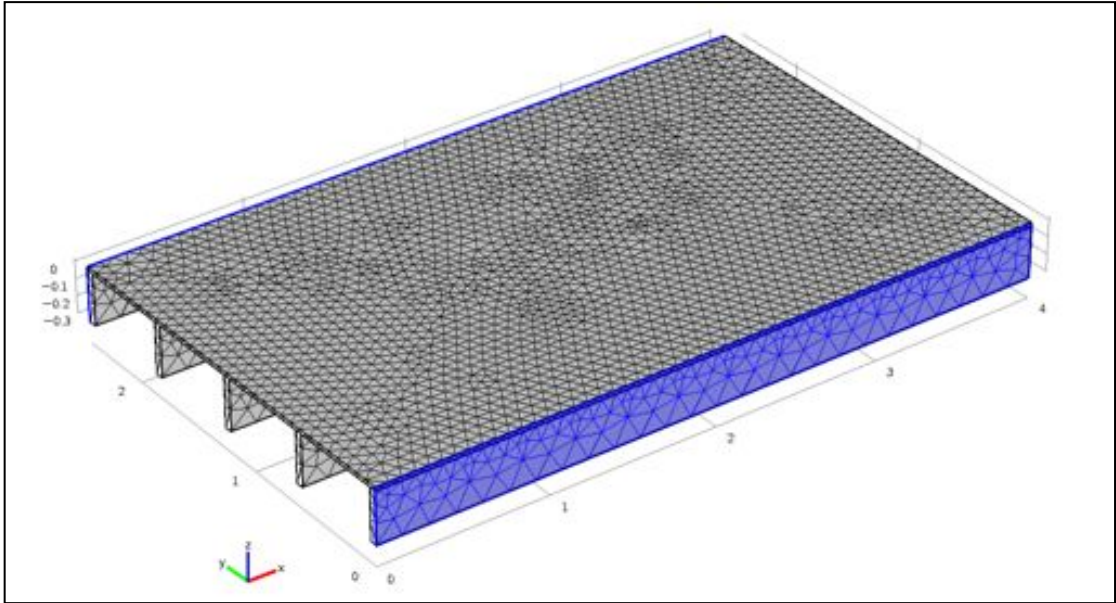


Figure 23 FEM mesh and constraint elements (view 1)

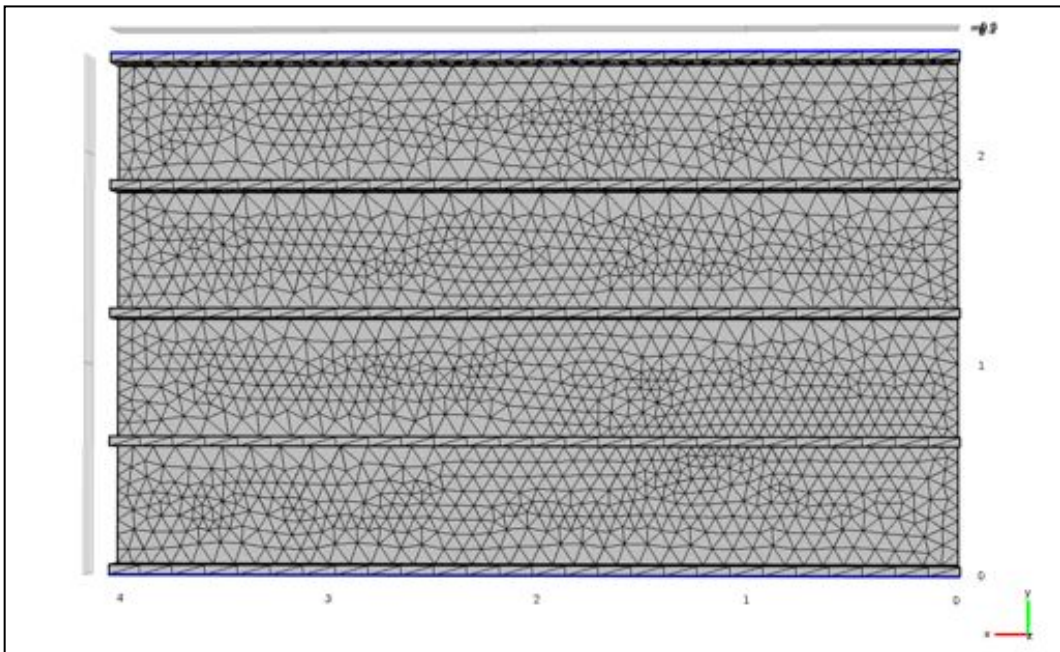


Figure 24 FEM mesh and constraint elements (view 2)

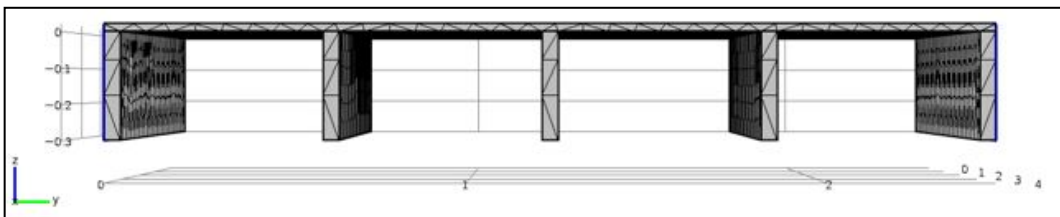


Figure 25 FEM mesh and constraint elements (view 3)

Table 14 WFEM / FEM frequency deviation (%) at eigenfrequencies

k_n [1/m]	Deviation [%]					
	BW 01	BW 02	BW 03	BW 04	BW 05	BW 06
/L	10	3	0	-2	-3	-2
2 /L	0	1	3	-8	-5	-3
3 /L	0	1	-3	-10	-8	-9
4 /L	-1	-6	-4	-9	-10	-10

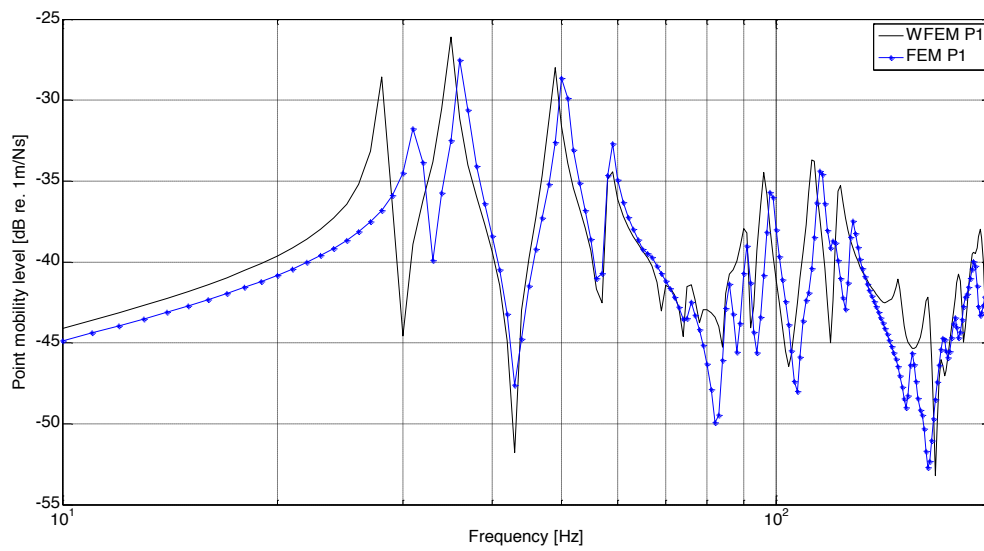


Figure 26 WFEM / FEM comparison for P1

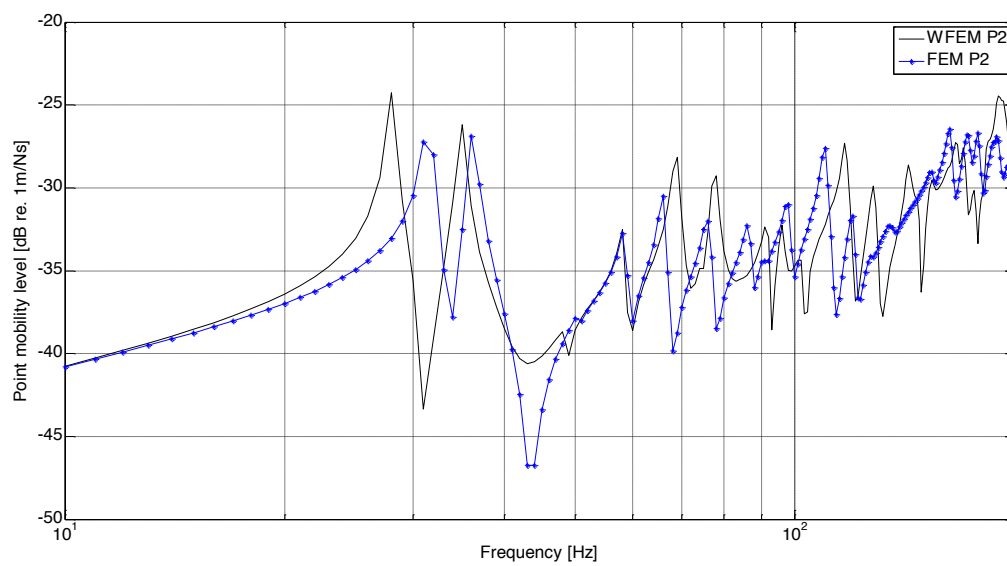


Figure 27 WFEM / FEM comparison for P2

4 Parameter study

This study consists in changing some of the main parameters of the LWF model to analyze the influence in the results. While designing the experiment, we decided to always keep the same bending waves sound velocity (c_B) for all the different scenarios. Thus, we could change the value of any parameter but " c_B " should be kept constant for all cases. Equation (11) has been used to calculate the bending wave sound velocity:

$$c_B = \sqrt{\omega} \left(\sqrt[4]{\frac{B}{\rho S}} \right) \quad (11)$$

ω , angular frequency [rad/s]

B , bending stiffness [kg·m], equal to the product of the Young Modulus (E) and the inertia moment (I)

ρ , density of the material [kg/m³]

S , cross section area [m²]

The parameter study has mainly focused in two different approaches that will be referred as PS_1 and PS_2. The first one consists in changing the elastic properties of the top board material. Basically, we have changed the Young's Modulus (E) and the density (ρ) to make the material more and less stiff than the original case. These two scenarios will be indicated as "PS_1.1 (less stiff)" and "PS_1.2 (stiffer)". For the second approach we have changed the cross section geometry of the beams and since we wanted to keep " c_B " constant we also had to change the Young's Modulus (E) and/or the density (ρ) values. Two scenarios have been analyzed and will be referred as "PS_2.1" and "PS_2.2" from now on.

The last section of this chapter includes an extra study where the original LWF has been compared with the vibrational response of the same floor but removing the beams, i.e. only the top board. This study has been included to check if the periodic nature of the LWF produces the well-know "Pass-band / Stop-band effect" (7)(8)(9)(10)(11).

4.1 Material's elastic constants analysis (PS_1)

As we have already said, this first case consists in changing the elastic properties of the top board of the LWF. *Table 15* shows the values of the parameters for the two evaluated scenarios plus the original one.

Table 15 Parameter values PS_1

Scenario	Original	PS_1.1 (less stiff)	PS_1.2 (stiffer)
E [N/m ²]	3.4 10 ⁹	1.7 10 ⁹	6.8 10 ⁹
[kg/m ³]	710	355	1420

Figure 28 and Figure 29 show the dispersion relation comparison between the original case and the new scenarios. These graphs give information of how the modal eigenfrequencies are shifted for the given scenarios.

More detailed information is given in Appendix C, where some deformation plots have been included, together with the dispersion relations plots of each bending wave separately, making the analysis easier.

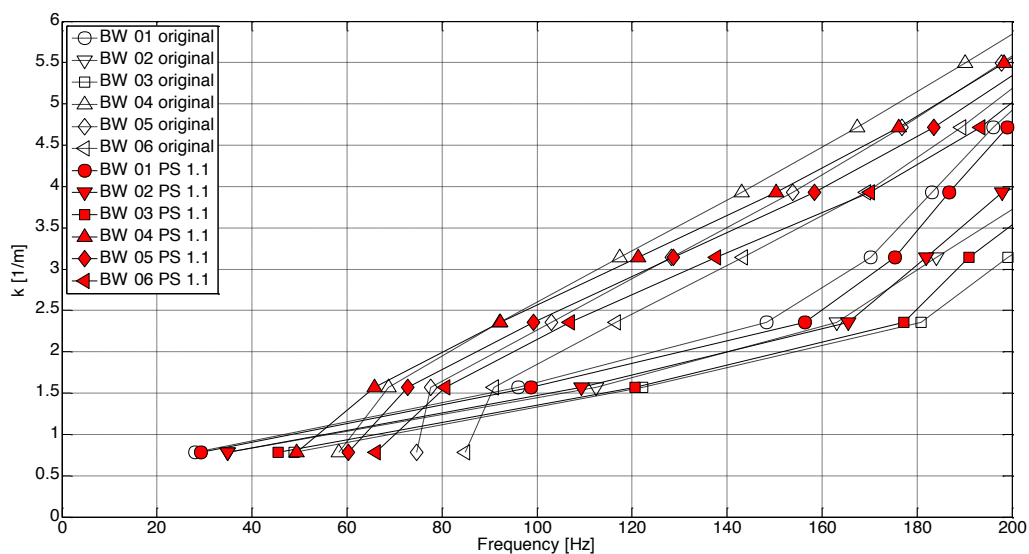


Figure 28 Modal dispersion relation comparison PS 1.1 (less stiff)

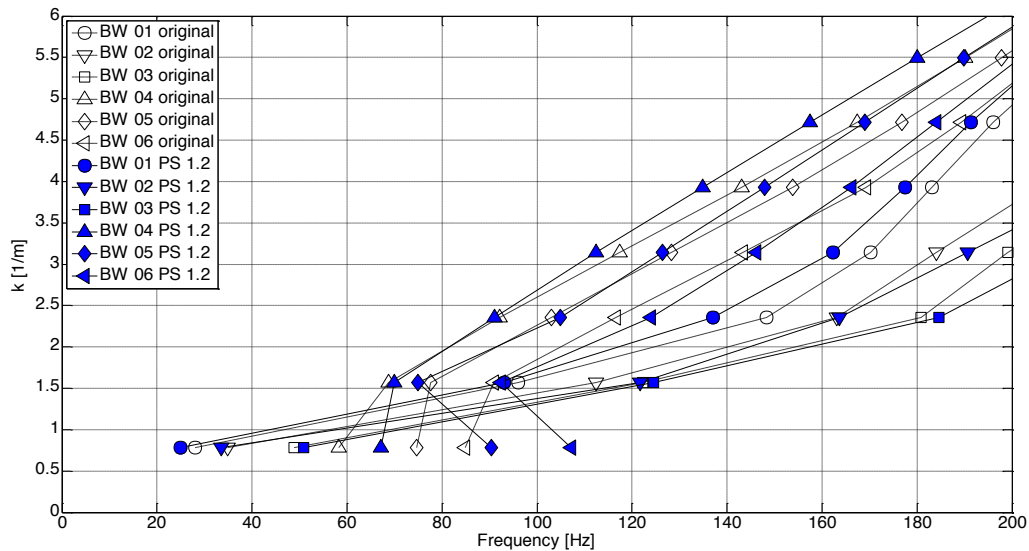


Figure 29 Modal dispersion relation comparison PS 1.2 (stiffer)

4.2 Geometry analysis (PS_2)

The second approach was to change the geometry of the LWF's beams. Two scenarios have been analyzed⁴ PS_2.1 and PS_2.2 that will be presented separately in the next sections.

4.2.1 Scenario PS_2.1

For the first scenario we have analyzed the dispersion relations differences when the floor is modelled with shorter (Z-dimension) and wider (Y-dimension) beams (see Figure 30) than the original case. The data used in the model and the original values are presented in the Table 16.

Table 16 Parameter values PS_2.1

Scenario	Original	PS_2.1
E [N/m ²]	3.4 10 ⁹	1.76 10 ¹⁰
[kg/m ³]	710	560
Beam height [m]	0.3	0.15
Beam width [m]	0.045	0.09

⁴ The calculations for the parameter study PS_2 have been done using the low resolution finite element model since we are only interested in the relative differences between them.



Figure 30 Geometry detail PS 2.1

The dispersion relations results have been divided for more clarity in two sets of waves. Set 1 BW01, BW02 and BW03 (Figure 31), and set 2 BW04, BW05 and BW06 (Figure 32). The first set of waves show a similar tendency for both scenarios while for the second set of waves the change is much more significant.

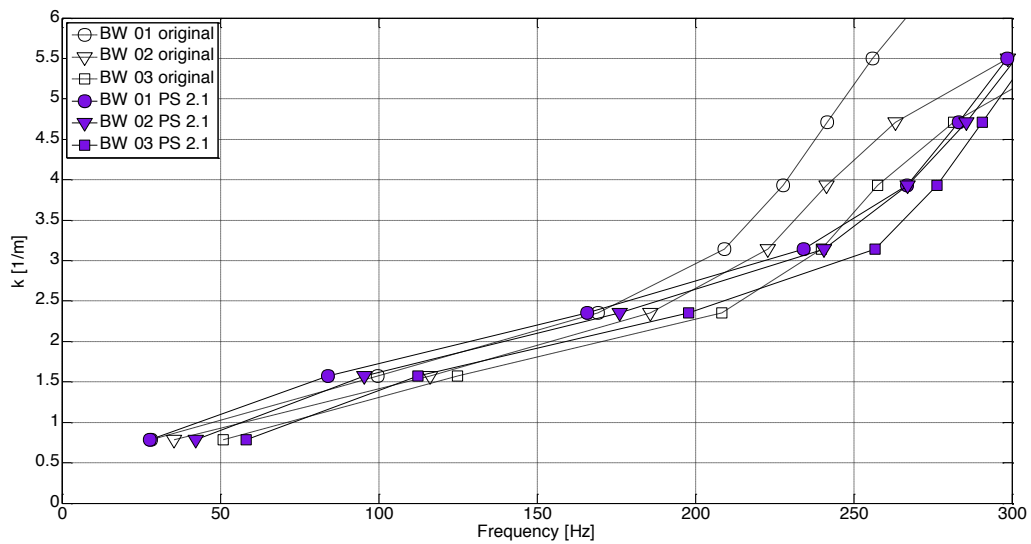


Figure 31 Modal dispersion relation comparison PS_2.1 for bending waves 1, 2 and 3

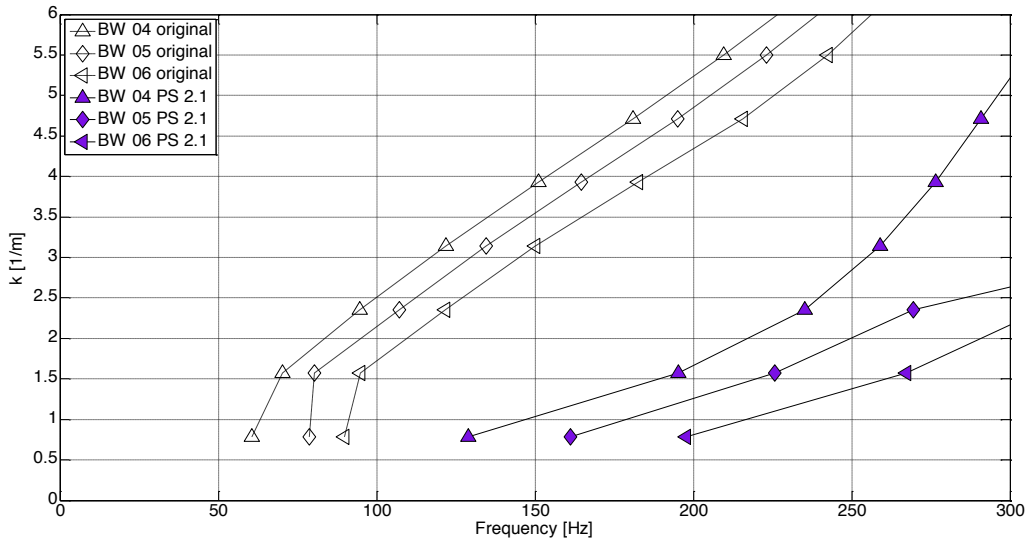


Figure 32 Modal dispersion relation comparison PS_2.1 for bending waves 4, 5 and 6

4.2.2 Scenario PS_2.2

In this second scenario, the beams have almost disappeared and the structure is getting closer to a simple plate. The geometry and data used for this case are given in Table 17 and Figure 33.

Figure 34 shows the dispersion relations results. It can be seen how the new structure has a similar behaviour as the one of the HWF (see Figure 17, only BW), a plate performance.

Table 17 Parameter values PS_2.2

Scenario	Original	PS_2.2
E [N/m ²]	3.4 10 ⁹	8.8 10 ⁸
[kg/m ³]	710	112
Beam height [m]	0.3	0.03
Beam width [m]	0.045	0.225



Figure 33 Geometry detail PS 2.2

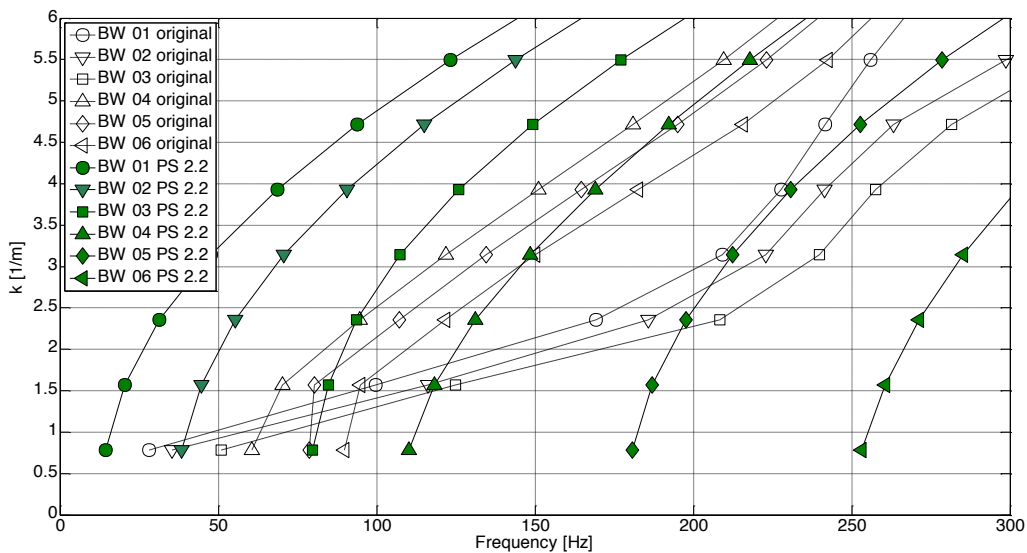


Figure 34 Modal dispersion relation comparison PS 2.2

4.3 Pass-band / Stop-band effect

This study is a continuation of the last section since we have done an extreme geometry change of the original floor's cross section, although in this case the elastic parameters have not change from the original case. The geometrical modifications have consisted in removing the beams from the original LWF. Therefore, the new structure is made up only of the top board of the LWF (LW plate). Although, it is not quite right since the systems are not completely comparable (p.e., stiffness of both systems are not the same), our opinion is that the comparison shows somehow the well known "Pass-band / Stop-band filtering effect" of a periodic lightweight system.

Figure 35 shows the results of the dispersion relations for the case of an infinite waveguide. For high wave numbers (>6-8 [1/m]), the figure shows how different sets of propagating bending waves of the original LWF

converge to the same line which can be considered the “pass-band filter”. If the systems were completely comparable, the lines should converge with a certain wave of the LW plate.

The first set of propagating waves of the original LWF should converge approximately with the 4th wave of the LW plate, the second set with the 8th, the third with the 12th and so on. This is known as PASS-BAND behaviour, while the LW plate waves 1-2-3/4-6-7/9-10-11, etc. would be the STOP-BAND effect of the periodic system (shown in Figure 35).

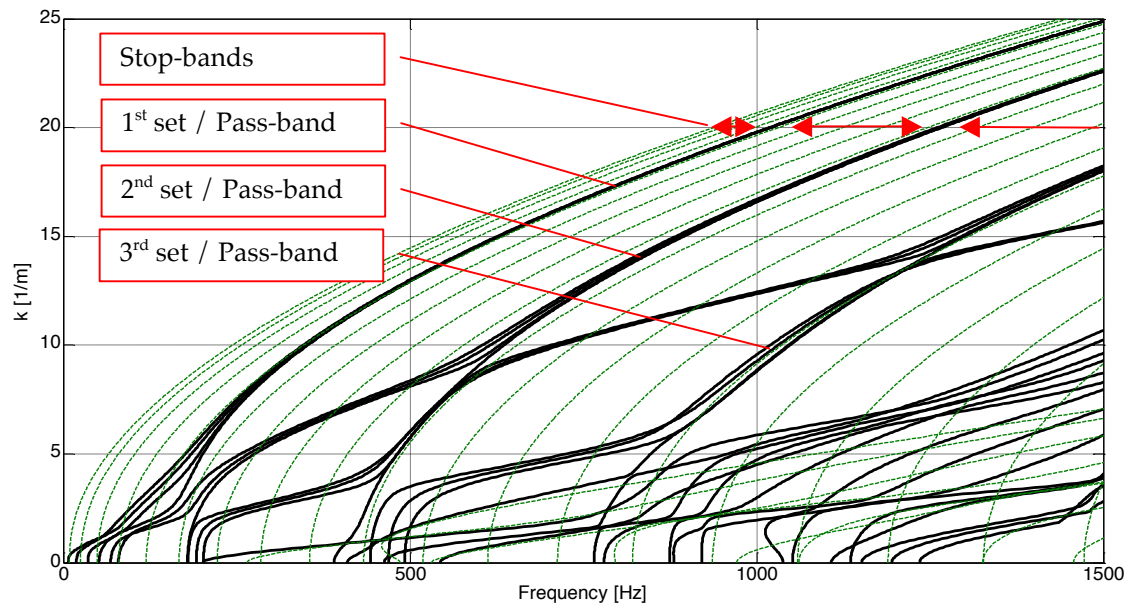


Figure 35 Dispersion relations comparison of the original LWF and the LW panel (infinite waveguide). Dotted green lines LW panel – Black lines Original LWF

This behaviour is related with the number and dimensions of the periodic bays between beams of the LWF, i.e. with the natural frequency of a single element (bay) of the LWF(12).

Figure 36, Figure 37 and Figure 38 show some examples of the cross-section deformation between the original LWF and the LW plate. It can be seen how an integer number of wavelengths must fit in the space between two beams: the first set of bending waves of the LWF corresponds with half wavelength, the second with one wavelength and the third with one and a half wavelength. Approximately, those set of waves correspond with the 4th, 8th and 12th bending wave of the LW plate (multiples of the number of bays of the LWF (4)).

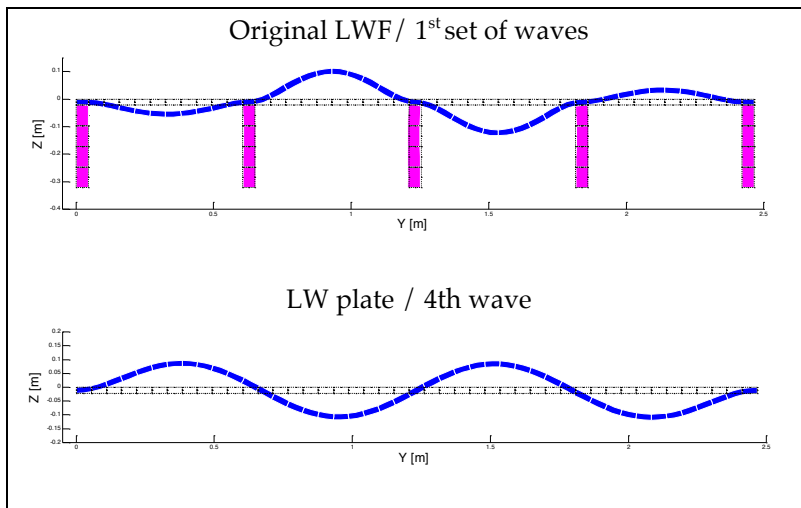


Figure 36 Cross section deformation comparison: 1st set of waves - 4th wave

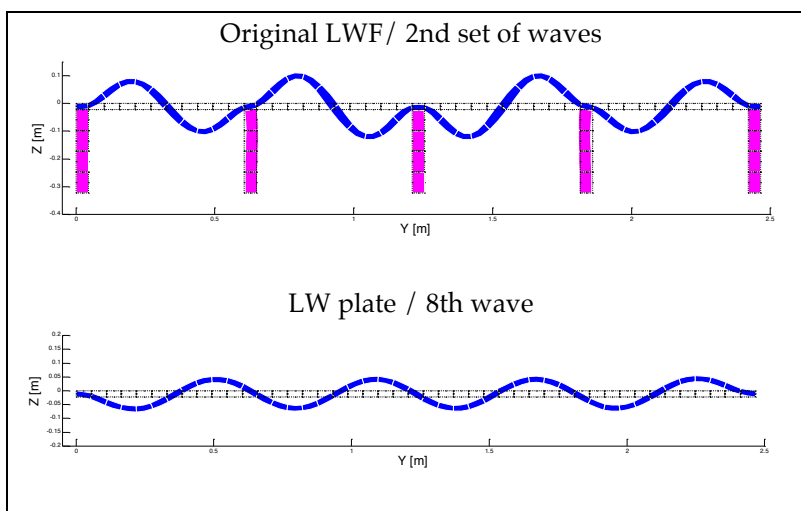


Figure 37 Cross section deformation comparison: 2nd set of waves - 8th wave

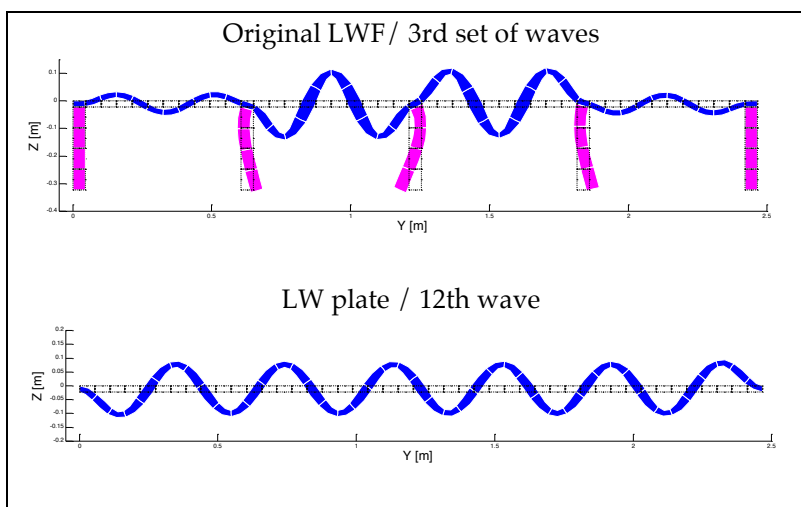


Figure 38 Cross section deformation comparison: 3rd set of waves - 12th wave

5 Sound radiation

The radiated sound power level and the radiation efficiency have been calculated when a unit point force is applied at points P1 (on beam) and P2 (between beams) of the LWF (see Figure 19).

The top surface of the LWF is assumed to be a “Plane, baffle radiator” which velocity field has been already calculated when it is excited at those points. The surface has been meshed to have a number of discrete point sources, each of them having its own volume velocity. The centre of the floor is now the origin of the coordinate system.

Once we have assigned the volume velocity to each point source, the sound pressure from each source to any receiving point can be evaluated by using Equation (7) and from those evaluations we can calculate the radiated sound power if enough number of receiving points are selected.

An overall of 300 point sources over the floor surface and 87 receiving points over a hemisphere surface have been used in our calculations. The set-up is shown in Figure 39.

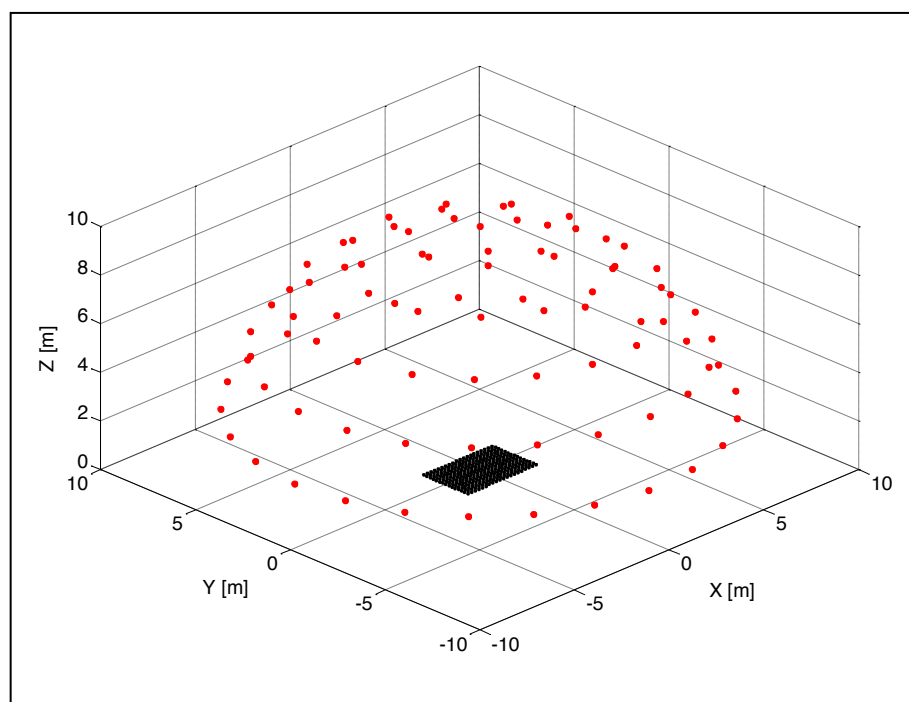


Figure 39 Detail of floor and hemisphere receiving points

For every receiving point the contribution to the sound pressure from each point source has been summed up and from the overall sound pressure of each receiving point the radiated sound power level has been calculated using Equation (9). Finally, the radiation efficiency has been determined by using Equation (10).

The results comparing both excitation positions (P1 and P2) are shown in Figure 40 and Figure 41.

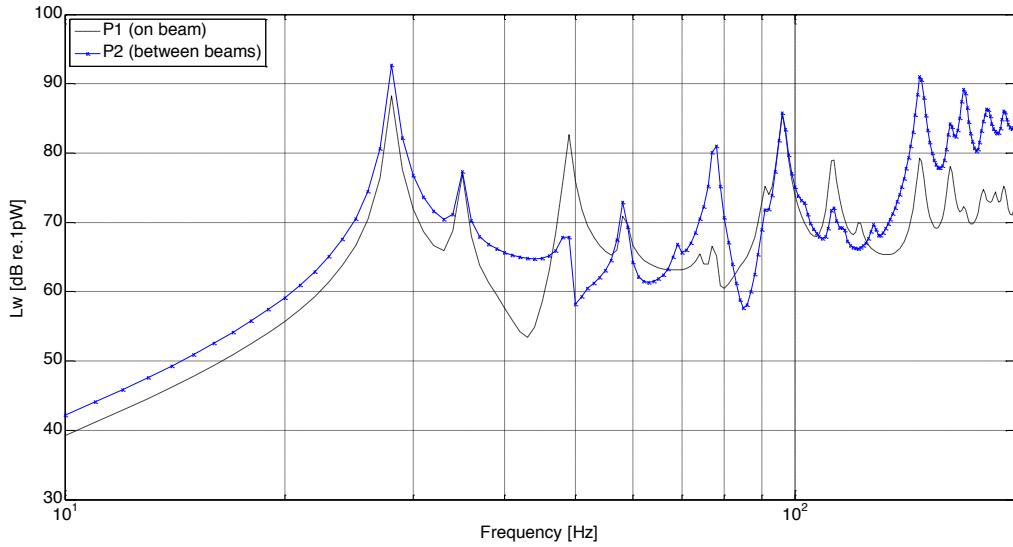


Figure 40 Radiated sound power exciting the floor at points P1 and P2

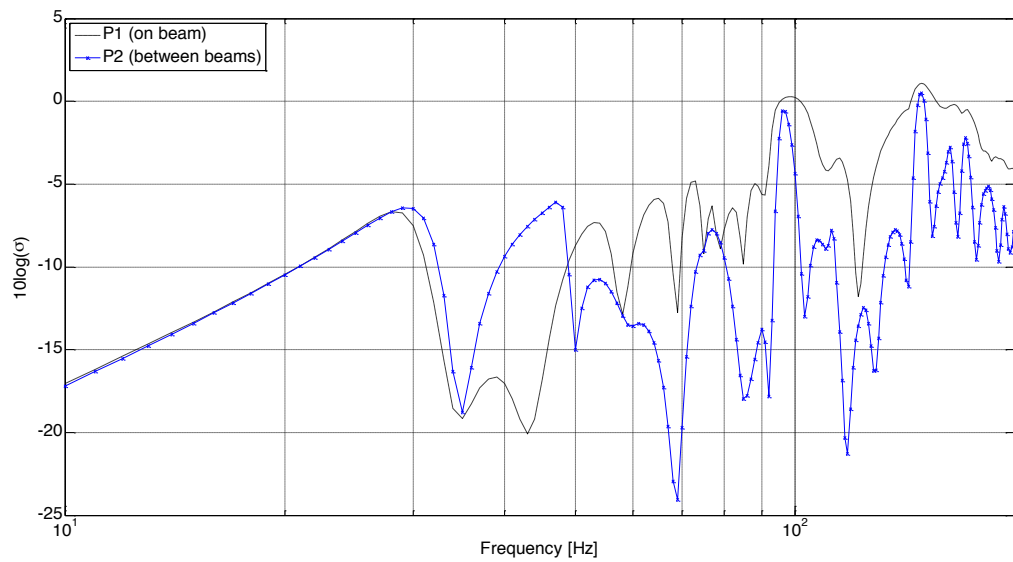


Figure 41 Radiation efficiency exciting the floor at points P1 and P2

Table 18 shows the values of the main “peaks” (frequency and sound power level) from Figure 40. The table includes an indication of which bending wave is responsible of each peak.

Table 18 Analysis of the “peaks” of the radiated sound power level

Excitation point	“Peak” Freq. [Hz]	“Peak” L_w [dB re. 1pW]	Bending wave
P1 (on beam)	28	88	BW01

	49	82	BW03
	96	86	BW01
	112	78	BW02
	148	79	BW01
	164	77	BW02
P2 (between beams)	28	93	BW01
	96	86	BW01
	148	91	BW01
	170	89	BW01

When the floor is excited at the point situated between the beams, the radiated power is higher than when it is excited on a beam. The main conclusion from analyzing the data presented in *Table 18* is how the first bending wave (BW01) is mainly responsible of the sound radiation in the analyzed frequency range.

From all the radiating peaks, it is important to highlight those at 96 Hz and 148 Hz since they have the higher radiation efficiency and they appear in both excitation cases.

6 Conclusions

The initial goals of this work were to gain a better understanding of the acoustical performance of a simple LWF and the evaluation of Waveguide Finite Element Method “WFEM” as a tool to predict the acoustic performance of structures. Therefore, we have drawn some conclusions based on the use of WFEM during the study and some others from the acoustic performance of the analyzed floors.

The conclusions drawn from using WFEM are considered below:

1. The main benefit of this method is that allows keeping the study from a “waves” point of view, what we consider basic for the physical understanding of the acoustical performance of a structure. We have used the tool to get dispersion relations, classify the type of waves, calculate mobilities, plot deformations, evaluate the sound radiation, etc. and in every case it is possible to find the corresponding wave, responsible of a specific acoustical performance. Furthermore, we could modify the properties of the structure and see how each specific wave changed.
2. In Chapter 3, we could see how the difference between the number of elements and DoF’s used for modeling the same structure using WFEM and normal FEM is enormous. This can be seen as an indicator of the computational effort needed for both cases. If the WFEM tools are optimized the method is much faster and requires much less computational effort than normal FEM tools.
3. In the other hand, we have seen how the method is limited (at least with the simplicity used during this work) to structures with constant properties along the waveguide, it is limited to the same loss factor for the whole structure (when calculating mobilities) and may be hard to implement complex boundary conditions.

Relative to the acoustical performance of the LWF the next conclusions are drawn:

4. At low frequencies, the results have shown how the vibrational field of the LWF is more complex than the one of the HWF. More complex means that there are more waves propagating in a LWF than in the HWF and the mobility level differences between both floors are huge.
5. From the comparison of the deformations plots of both floors, we have seen how, the “plate behavior” of the HWF, happens in the low order bending waves of the LWF for the first wavenumbers but disappears for greater values. The LWF is a lightweight plate with periodic beams in one dimension. This type of periodic structures has been deeply studied and they are characterized by a periodic pass-band / stop-band filter behavior as it has been shown in Section 4.3.
6. Some additional scenarios have been analyzed by changing some properties of the original LWF. The effect of changing the elastic properties of the top board and the influence of the beams when they are made shorter to the point of disappearing have been shown. Again, the most important conclusion is that we can analyze the influence of the changes in each individual propagating wave.
7. The overall radiated power is higher when the floor is excited at a bay between two beams. When the sound radiation results are correlated to

the propagating bending waves it is shown how the first bending wave (BW01) is mainly responsible of the sound radiation of the LWF. Particularly, those resonances at 96 Hz and 148 Hz are of special interest since they present the higher radiation efficiency and they appear in both excitation cases.

7 Future work

The results of this work should be validated using experimental measurements. This was the initial plan but after two failed tries it was discarded.

The radiation of the parameter study scenarios must be calculated and the results compared with those of the original LWF. The influence of the parameters in the sound radiation must be studied.

Moreover, the excitation used in the whole study has been a unit point force. In the future, different and more realistic excitations (p.e. a falling mass, footsteps,...) should be included and compared with the results of normalized experiments.

Finally, some of the steps of the WFEM process, as the geometry design, the calculations to get the deformation plots, etc., should be optimized because even if the method requires less computational effort than a FEM calculation of a complete 3D structure sometimes takes longer time just because the process is not completely optimized.

8 References

1. **Hagberg, K.** *Evaluation of sound insulation in the field.* Lund University. Lund : s.n., 2005. Licentiate thesis. report TVBA 3127, ISSN 0281-8477.
2. *Acoustics -- Measurement of sound insulation in buildings and of building elements -- Part 7: Field measurements of impact sound insulation of floors.* 1998. ISO 140-7.
3. **Skökvist, Lars-Göran.** *Structural Sound Transmission and attenuation in lightweight structures.* Göteborg : Division of Applied Acoustics - Department of Civil and Environmental Engineering - Chalmers University of Technology, 2008.
4. **B., Aalami.** Waves in prismatic guides of arbitrary cross section. 1973, pp. p.1067-1071.
5. **Sabiniaz, Patrick.** *On the waveguide finite element method for modelling vibrations : general investigation and application to a car tyre.* Göteborg : Chalmers University of Technology, 2004.
6. **Cremer, L., Helckl, M. and Petersson, B.A.T.** *Structure-Borne sound.* 3rd. Berlin : Springer, 2005.
7. **Brillouin, L.** *Wave propagation in periodic structures.* s.l. : Dover Publications, 1953.
8. *Wave beaming and wave propagation in light weight plates with truss-like cores.* **Kohrs, Torsten and Peterson, Björn A.T.** 321, s.l. : Journal of Sound and Vibration, 2009, pp. 137–165.
9. *Wave propagation in light weight profiles with truss-like cores: Wave number content, forced response and influence of periodicity perturbations.* **Kohrs, Torsten and Peterson, Björn A.T.** s.l. : Journal of Sound and Vibration, 2006.
10. *Passive vibration control.* **Mead, Denys J.** s.l. : Wiley, 1999.
11. **Cremer, L. and Leilich, H.O.** On Theory of flexural periodic systems. s.l. : Archiv der Elektrischen Übertragung 7, 1953.
12. *Wave propagation and natural modes in periodic systems: Mono-coupled systems.* **Mead, D.J.** s.l. : Journal of Sound and Vibration, 1975.

Appendix A. Dispersion relations frequencies

k_n [1/m]	Frequency [Hz]					
	BW 01		BW 02		BW 03	
	HWF	LWF	HWF	LWF	HWF	LWF
/L	175	28	419	35	730	49
2 /L	231	96	471	112	778	122
3 /L	339	148	563	163	859	181
4 /L	492	170	695	184	974	199
5 /L	679	183	859	206	1119	221
6 /L	890	196	1051	240	1289	253
7 /L	1119	211	1263	286	1481	295
8 /L	1360	228	1490	338	1690	347

k_n [1/m]	Frequency [Hz]					
	BW 04		BW 05		BW 06	
	HWF	LWF	HWF	LWF	HWF	LWF
/L	1085	58	1471	75	1878	85
2 /L	1129	69	1510	78	1913	91
3 /L	1201	92	1574	103	1971	117
4 /L	1302	117	1664	128	2052	143
5 /L	1430	143	1779	154	2155	169
6 /L	1582	167	1915	177	2277	189
7 /L	1755	190	2136	198	2419	207
8 /L	1946	213	2377	219	2792	225